Journal Pre-proofs

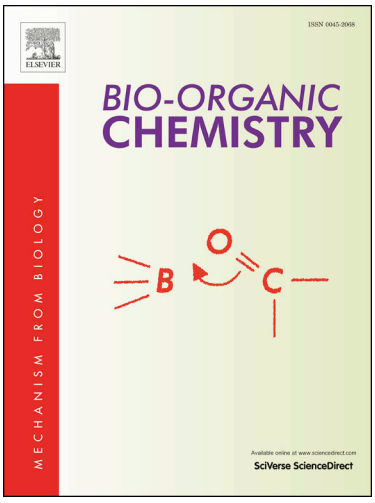

Functional interplay between short antimicrobial peptides and model lipid membranes

Lorena Gratino, Marta Gogliettino, Marco Balestrieri, Alessandra Porritiello, Principia Dardano, Bruno Miranda, Rosa Luisa Ambrosio, Monica Ambrosio, Luigi Nicolais, Gianna Palmieri

PII: S0045-2068(24)00844-7
DOI: https://doi.org/10.1016/j.bioorg.2024.107939
Reference: YBIOO 107939

To appear in: *Bioorganic Chemistry*

Received Date: 18 July 2024
Revised Date: 30 October 2024
Accepted Date: 1 November 2024

Please cite this article as: L. Gratino, M. Gogliettino, M. Balestrieri, A. Porritiello, P. Dardano, B. Miranda, R. Luisa Ambrosio, M. Ambrosio, L. Nicolais, G. Palmieri, Functional interplay between short antimicrobial peptides and model lipid membranes, *Bioorganic Chemistry* (2024), doi: https://doi.org/10.1016/j.bioorg.2024.107939

This is a PDF file of an article that has undergone enhancements after acceptance, such as the addition of a cover page and metadata, and formatting for readability, but it is not yet the definitive version of record. This version will undergo additional copyediting, typesetting and review before it is published in its final form, but we are providing this version to give early visibility of the article. Please note that, during the production process, errors may be discovered which could affect the content, and all legal disclaimers that apply to the journal pertain.

© 2024 Published by Elsevier Inc.

Journal Pre-proofs

Functional interplay between short antimicrobial peptides and model lipid membranes

Lorena Gratino[a,1], Marta Gogliettino[a,1], Marco Balestrieri[a,*], Alessandra Porritiello[a], Principia Dardano[b], Bruno Miranda[b], Rosa Luisa Ambrosio[c], Monica Ambrosio[a], Luigi Nicolais[d], and Gianna Palmieri[a,d,*]

a ***Institute of Biosciences and BioResources - National Research Council (IBBR-CNR), 80131 Napoli, Italy***

b ***Institute of Applied Sciences and Intelligent Systems - National Research Council (ISASI-CNR), 80131 Napoli, Italy***

c ***Department of Veterinary Medicine and Animal Production, University of Naples Federico II, Naples, Italy***

d ***Materias Srl, 80146 Naples, Italy***

* **Corresponding authors.**

E-mail address: **gianna.palmieri@ibbr.cnr.it (G. Palmieri), marco.balestrieri@ibbr.cnr.it (M. Balestrieri)**

[1] **These authors contributed equally to this work**

Journal Pre-proofs

ABSTRACT

Antimicrobial peptides (AMPs) are considered an attractive generation of novel antibiotics due to their advantageous properties such as a broad spectrum of antimicrobial activity against pathogens, low cytotoxicity, and drug resistance. Although they have common structural features and it has been widely demonstrated that bacterial membranes represent the main target of the peptide activity, the exact mechanism underlying the membrane perturbation by AMPs is not fully understood. Nevertheless, all the proposed modes of action implicate the preliminary interaction of AMPs with the negatively charged lipids in bacterial membranes. Recently, the structural and functional characterization of two AMPs, RiLK1 and RiLK3, was reported. Specifically, both peptides were revealed to be multitalented compounds capable of binding Gram-positive and Gram-negative liposome models with high affinity, but their mechanism of action remains elusive. In this paper, the effects of RiLK1 and RiLK3 on vesicles mimicking prokaryotic and eukaryotic cell membranes were further examined by using different approaches. Fluorescence and quenching assays either by acrylamide or lipophilic probes suggested that the peptides were mainly located at the interface of the negatively charged membranes that mimicked those of *Salmonella* Typhimurium and *Staphylococcus aureus*, possibly oriented in a parallel manner. Furthermore, RiLK1 and RiLK3 caused a significant leakage of carboxyfluorescein from bacterial liposomes, demonstrating that they can permeabilize the target membranes at high doses. Conversely, both peptides appear to behave

like cell penetrating peptides (CPPs) at concentrations near their MIC values evaluated against the bacterial targets. Moreover, Dynamic Light Scattering provided further insights on the mechanisms of antimicrobial peptide against the bacterial liposomes. Conclusively, *in vitro* experiments indicated that RiLK1 and RiLK3 displayed potent bacteriostatic efficacy at low micromolar concentrations against an antibiotic-resistant ESKAPE pathogen, making them a valuable tool in preventing and treating infections caused by such bacteria.

***Keywords*: Antimicrobial peptide; Fluorescence spectroscopy; Liposome; ESKAPE pathogen; Dynamic Light Scattering**

Journal Pre-proofs

[1] **Abbreviations**: PC, phosphatidylcholine; SM, sphingomyelin; PS, phosphatidylserine; DOPE, dioleoyl-phosphatidylethanolamine; POPE, palmito-yl-oleoyl-phosphatidylethanolamine; POPG, palmitoyl-oleoyl-phosphatidylglycerol; CL, cardiolipin

1. Introduction

Antimicrobial peptides (AMPs) are amino acid sequences, belonging to the innate immune system [**1-2**] of animals and plants and are promising candidates for new antibiotic therapeutics [**3-6**]. Although AMPs are characterized by no conserved sequence motifs, most of them are short, cationic, and amphipathic, with a large conformational flexibility and an undefined secondary structure in water. These compounds have a broad spectrum of activity against pathogens such as bacteria, viruses, fungi, and parasites and show diverse mechanisms of action that may help to prevent the development of resistance processes, making them attractive candidates to fight antibiotic-resistant infections **[7,8]**. Therefore, naturally occurring AMPs, their mutants, and newly designed peptides are intensively screened as potential therapeutic agents **[4,5,7]**.

AMPs generally target and bind bacterial membranes via peptide-lipid interactions or, in a few cases, cross the cell membrane and access intracellular compartments, interacting with intracellular molecules (RNA, DNA, and proteins) **[9]**. Several studies have shown that AMPs can disrupt cell membranes by different mechanisms, leading to membrane permeabilization and cell death [**9-11**]. The membrane AMP interaction mostly involves electrostatic potentials, secondary structures, and lipid bilayer insertion, which can be affected by the lipid chain length and saturation. The composition of lipid membranes can significantly impact the secondary structures of AMPs, stabilizing α-helical conformations, β-sheet, or extended secondary structure motifs in specific lipid environments [**12**]. The peptides typically cause leakage of the cell membranes by accumulating on their external surface, inserting below the lipid headgroups parallel to the membrane surface, and perturbing the surface tension of the outer lipid leaflet [**13**]. When the bound peptide exceeds a critical value, defects are formed to release the accumulated stress. This mechanism of action is identified as the "carpet" model considering that the threshold for defect formation requires a high coverage of the bilayer surface by bound peptides [**14**]. In the barrel-stave alternative model of transmembrane pores formation, peptides first bind to the membrane surface, then insert in a trans bilayer orientation combining like the staves in a barrel and forming a channel in the bilayer. In this case, the threshold of membrane-bound peptides required for pore formation can be lower than that needed for AMPs according to the carpet model mechanism [**13,15**].

Model membrane systems, including liposomes, have been used to study mechanisms of action and explore the effect of peptides on the structure of the lipid bilayers [**9**]. Although they are less complex than bacterial membranes, model membranes are suitable for investigating specific cell wall components and membrane-lipid interaction of AMPs, which is crucial for developing alternative antimicrobial strategies to counteract bacterial resistance to antibacterial drugs [**16,17**]. Liposomes are considered versatile, easy to prepare, and very useful model membranes, as they can be obtained with well-defined lipid compositions, biophysical properties, and conditions lowering the variables existing in biological assays.

This work was focused on two short cationic and amphipathic peptides, RiLK1 (RLKWVRIWRR-NH_2) and its derivative RiLK3 (RLRWVRIWRR-NH_2), where the lysine is

replaced with an arginine residue, which can represent simple models of AMPs to gain insights into the mechanisms of membrane permeabilization and antibacterial activity.

The two 10-amino acid molecules were previously designed based on the bactericidal and antibiofilm peptide 1018-K6 [**18,19**], derived from a bovine HDP (host defense peptide) bactenecin belonging to the cathelicidins' family [**20**]. Previous structural and functional investigations revealed that RiLK1 and RiLK3 were multitalented compounds, being active against fungi, viruses, Gram-positive and Gram-negative bacteria at low micromolar ranges, with no cytotoxic effects on human cells [**21-23**]. Moreover, results evidenced that in aqueous solutions, the two peptides adopt a random coil conformation, while in micellar solutions they aggregate showing a conformational propensity to self-assemble in regular structures and providing a possible explanation for their potent bactericidal, antifungal, and anti-biofilm activities [**21-23**]. Recently, it has been also demonstrated that RiLK1 and RiLK3 can bind Gram-positive and Gram-negative liposome models, nevertheless, the mechanistic basis of their bactericidal action against these bacteria is still not understood [**23**].

In this study, heterogeneous liposomes of two representative Gram-negative and Gram-positive bacteria, *Salmonella* Typhimurium, and *Staphylococcus aureus,* were used for in-depth analysis of RiLK1 and RiLK3 cell membrane interactions underlying their bactericidal activity. Specifically, by combining Dynamic Light Scattering (DLS) and fluorescent spectroscopy assays, the membranolytic action of the two peptides was explored to get a better understanding of the antimicrobial process and to evidence their differences in terms of selective properties and behaviours towards lipid vesicles, which mimic the outer surface of the bacterial and mammalian cell membranes.

In addition, both peptides were preliminary tested against the clinically isolated ESKAPE pathogen *Enterococccccus faecium,* a worldwide recognized Gram-negative antibiotic-resistance bacterium, which can lead to severe diseases in susceptible individuals, often associated with urinary tract infections, endocarditis, and bacteraemia although it is naturally part of the microbiota. *E. faecium* has revealed resistance to a panel of antibiotics commonly used such as penicillin, fluoroquinolones, macrolides, and tetracyclines. The development of vancomycin-resistant strains of *E. faecium* is also of considerable concern to healthcare specialists due to their excessive persistence in hospital locations and limited treatment options. In this scenario, the design of novel and alternative treatment strategies, which include the use of antimicrobial peptides to counter the global threat of multi-resistant enterococci is a serious challenge.

This work opens a promising road to discover the relationship among the sequences of antimicrobial peptides, the mechanism, and their target specificity, which is one of the key factors in the race to develop a suitable peptide-based antibiotic therapy, especially for combating drug-resistant bacterial infections.

2. Results and Discussion

2.1. Interaction of AMPs with the bacterial membranes

The interaction of antimicrobial peptides (AMPs) with lipid bilayers has been attracting the attention of a growing community of scientists for several years. The mode of action of these membranolytic peptides includes two main stages: first, the cationic AMPs selectively bind onto the surface of the negatively charged cell membranes and then disrupt bacterial membranes through different mechanisms. The binding event is considered the primary step involved in the mechanisms exhibited by most AMPs for killing and inhibiting the growth of bacteria [**24,25**]. Hence, to gain insight into the ability of our designed peptides (RiLK1 and RiLK3) to selectively target phospholipid membranes of differing compositions and to study their interaction with bacterial/mammalian membrane mimics, fluorescence spectroscopy was employed tacking advance the presence of two Trp residues in the peptide sequences [**21-23**]. Indeed, it is known that the fluorescence intensity of tryptophan and the shift to the lower wavelength (blue shift) are significantly increased when it is immersed into a more hydrophobic environment as occurs upon binding of Trp-containing peptide to lipid membranes [**26**].

In a preliminary study, it was demonstrated that RiLK1 bound to the negatively charged lipid vesicles of *Salmonella* Typhimurium ($DOPE_{78}$:$POPG_{18}$:CL_4) **[27,28]** and *Staphylococcus aureus* (CL_{42}:$POPG_{58}$) **[29,30].** with an affinity higher than that observed for its derivative RiLK3, while no binding for the uncharged lipids such as those of zwitterionic (PC) and eukaryotic (PC_{40}:$POPE_{40}$:SM_{15}:PS_5) membranes was detected with both molecules [**23**]. Based on these results, a more in-depth investigation of mechanisms by which RiLK1 and RiLK3 induced bacterial membrane perturbation was performed in this study.

Firstly, the changes in fluorescence intensity of the Trp residues of RiLK1 and RiLK3 as a function of lipid concentration were monitored. Concerning RiLK1, upon titrating with increasing micromolar concentrations of *Staphylococcus*-like vesicles, a detectable increase in the emission intensity was observed (the fluorescence emission increases 2.4 times to the free peptide), accompanied by a clear blue shift of the emission maxima of Trp (up to 14 nm), indicating that these residues were buried in a more hydrophobic environment preventing solvent exposure (**Fig. 1A**). A similar result was obtained upon the addition of increasing concentrations of *Salmonella* vesicles, although the fluorescence enhancement was less strong, and the blue shift went to saturation more slowly than that observed for *Staphylococcus* (**Fig. 1B**). These data suggested that RiLK1 was able to interact with both model membranes, although with different affinity and/or binding modes. Conversely, no significant variations (ranged from 2 nm to 4 nm) in the emission maxima (λmax) of Trp were observed upon titration with increasing concentrations of zwitterionic and eukaryotic mimicking model membranes (**Fig. 1C,D**), confirming the preference e selectivity of RiLK1 for the negatively charged membranes over the uncharged ones, probably because the mammalian membranes are deficient in anionic lipids, thus preventing AMPs to undergo a proper initial electrostatic interaction with them. The changes in the tryptophan fluorescence emission were plotted as a function of lipid concentration and reported in **Fig. 1E**. Similar trends and results were observed in the case of RiLK3-binding (**Fig. 2**).

2.2. Fluorescence quenching experiments

The titrations described above indicate that the peptides under investigation can interact with lipid membranes; however, another key factor in the determination of the mechanisms of membrane destabilisation by AMPs consists in their position inside the phospholipid bilayer architecture. In this regard, fluorescence quenching experiments can provide important

information on the insertion depth of peptides as changes in their orientation in the lipid bilayer can impact the fluorescence properties. To this aim, MLVs were used as model systems that could better represent the complexity of natural membranes, showing a structure like a matryoshka doll of concentric bilayers. Firstly, Trp fluorescence quenching experiments by the neutral water-soluble molecule acrylamide were conducted for RiLK1 and RiLK3, in the absence and presence of mammalian and bacterial mimetic membranes, and at increasing concentrations of the quencher (**Fig. 3**). Acrylamide has the advantage of no charge interactions with the headgroups of negatively charged lipids and it is often used to study the accessibility of peptide fluorophores in aqueous environments. If the fluorescent probe is fully shielded in the membrane, it becomes inaccessible to this aqueous quencher, possessing a low penetration capacity into lipid bilayers [**31**].

Data are reported in a so-called Stern–Volmer plot and the extent of quenching in fluorescence of the free peptides as well as the peptide-membrane mimic mixtures was expressed in terms of Stern-Volmer Constant (K_{SV}), whose reduction implies that the fluorophore is buried within the hydrophobic lipid core of the bilayer and indicates the extent of Trp's exposure to solution. As shown in **Fig. 3**, the tryptophan residues of both peptides were readily quenched in the buffer, evidencing that they are easily accessible in the aqueous solution such as in the presence of mammalian membranes. When RiLK1 (**Fig. 3A**) and RiLK3 (**Fig. 3B**) were in complex with bacterial mimicking MLVs, the tryptophan fluorescence was less affected by the acrylamide and decremented in a dose-dependent manner (**Fig. S1**).

From the quenching profiles, the K_{SV} constants were obtained as described in the Methods section. As reported in **Table 1**, the values of K_{SV} for both peptides are significantly lower in the presence of *S. aureus* and *S.* Typhimurium lipid vesicles than those in buffer solution, demonstrating that Trp residues become inaccessible for quenching by acrylamide, being buried into lipid bilayers. The linear behaviour of Stern-Volmer curve observed with both peptides and bacterial liposomes suggested also the existence of fluorescence populations oriented parallel to the membranes and then with the same accessibility to the quencher of Trp residues. Furthermore, the NAF (normalized accessibility factor), defined as the ratio between the Stern–Volmer constant in the presence and absence of MLV, was calculated to compare the peptides (**Table 1**). Specifically, an increased NAF value corresponds to higher Trp exposure to solvent, and inversely, a lower NAF value relates to its insertion in the lipid bilayer. The NAF of RiLK3 in both bacterial vesicles was lower than that observed for RiLK1 (**Table 1**), highlighting that RiLK3 is inserted deeper in the bilayer than RiLK1, whilst the tryptophan residues of RiLK1 can be located closer to the surface of bacterial membranes, resulting more accessible to acrylamide quenching. This behaviour could be explained by the increased number of Arg residues in RiLK3 respect to RiLK1, considering that the guanidinium group can form stronger and more extensive hydrogen bonds and electrostatic interactions with the negatively charged components of bacterial membranes.

These results also support the blue shifts observed for these peptides in the presence of the two bacterial lipid environments. In contrast, the higher K_{SV} values, calculated in the presence of vesicles with lipid compositions mimicking those of mammalian membranes (zwitterionic and eukarya), evidenced that RiLK1 and RiLK3 do not interact with the mammalian MLVs, consistently with the results obtained from the blue shift experiments (**Fig. 1 and Fig. 2**). It is worth noting that the K_{SV} values in the buffer solution were smaller than those detected with mammalian membranes, possibly due to the propensity of both peptides to self-assembling in regular structures, which strongly affected the quenching by acrylamide [**21-23**].

The decreased access of the aqueous quencher acrylamide to Trp upon the interaction of the peptides with lipid vesicles should be accompanied by increased accessibility to quenchers

present in the hydrocarbon phase of the bilayers. Therefore, to get more information on the in-depth location of RiLK1 and RiLK3 in the lipid membranes, the relative quenching of the Trp fluorescence was monitored by the lipophilic spin probes 5-doxyl-stearic acid (5-NS) and 16-doxyl-stearic acid (16-NS). These two derivatized stearic acids differ in the position of the quencher moiety (doxyl) along the hydrocarbon chain, thus allowing the assessment of the relative deepness of a peptide in the membrane. Specifically, the 5-NS probe is a better quencher for molecules near or to the membrane interface, whereas the 16-NS is more useful for molecules buried deeply in the bilayer [**32**].

The variation in the fluorescence intensity as a function of the concentration of both 5-NS and 16-NS quenchers is shown in **Fig. 4 and Fig. 5** and the corresponding K_{SV} values are presented in **Table 2**. Results evidenced that 16-NS quenched RiLK1 (**Fig. 4A,B**) and RiLK3 (**Fig. 5A, B**) less efficiently than 5-NS (**Fig. 4C,D** and **Fig. 5C,D**) in presence of both bacterial membranes, consistently with the location of the Trp residues near the membrane lipid/water interface in a shallow position. These findings agree with the results obtained using acrylamide, where it was found that a fraction of the peptide population was buried in the bilayer. The Stern–Volmer plots of RiLK1 and RiLK3 quenching resulting from the two lipophilic probes in the presence of *S. aureus* and *S.* Typhimurium MLVs are reported in **Fig. 4E,F** and **Fig. 5E,F**, respectively. It is worth noting that the Stern-Volmer curves are linear when 5-NS or 16-NS were used as quenchers with both peptides and *bacterial* membranes, revealing that RiLK1 and RiLK3 were oriented parallel to the surfaces.

2.3. The effects of RiLK1 and RiLK3 on membrane permeability

Bilayer disruption is commonly proposed to play a key role in the mechanism of action of many antimicrobial peptides [**25,33**]. Therefore, to evaluate if RiLK1 and RiLK3 could permeate bacterial membranes, their effects on the release of the encapsulated fluorophores 5-carboxyfluorescein (CF) were studied. To this aim, large unilamellar vesicles (LUVs), whose lipid composition mimics *Salmonella* and *Staphylococcus,* were prepared with 25 mM CF, a concentration at which the dye fluorescence is self-quenched. Thus, the bilayers' liposomal leakage and membrane permeability upon interaction with RiLK1 or RiLK3 at 15 μM and 30 μM concentrations were followed through the increase in the fluorescence intensity of CF released to the surrounding medium. Full release (100%) was established by adding the detergent Triton X-100 to the mixture after the 30-minute course.

As shown in **Fig. 6**, RiLK1 and RiLK3 exhibited permeabilization properties against both LUVs mimicking *Salmonella* (**Fig. 6A**) and *Staphylococcus* (**Fig. 6B**) membranes at 30 μM concentration, as evidenced by the induced CF release, although with different extents. Specifically, RiLK1 caused a very fast CF leakage and showed a higher membrane perturbation potency with almost a complete release of the content from *Salmonella* (95%) LUVs (**Fig. 6A**) compared to *Staphylococcus* membranes (54%) (**Fig. 6B**).This different behaviour could be due to the distinct lipid compositions and surface charge of the two membrane models [**23**].

The partial de-structuration, evidenced by RiLK1 following the interaction with *Staphylococcus* membranes, may be due to a competition between electrostatic and hydrophobic forces. Indeed, in the case of membranes consisting of zwitterionic phospholipids such as those of *Salmonella*,

RiLK1 could be inserted more deeply into the hydrophobic part of the bilayer (through the hydrophobic peptide face containing the Trp residues) causing a severe leakage. In contrast, the negatively charged lipids such as those of *Staphylococcus,* could exert an electrostatic attraction versus the peptide, inhibiting its deeper insertion and resulting "blocked" into the lipid headgroup region. This is in line with the data obtained by the fluorescence quenching experiments with the lipophilic spin probes 5-NS and 16-NS. On the other hand, the effects observed for RiLK3 were comparable when both bacterial model membranes (maximum leakage 74%) were used, thus suggesting that this peptide could damage the membranes of Gram-positive and Gram-negative bacteria *via* similar mechanisms (**Fig. 6A,B**).

Conversely, the behaviour of both peptides against *Staphylococcus*-like membranes appeared different at lower concentrations (near their MIC values), evidencing that these AMPs did not induce cell membrane damage under these conditions (**Fig. 6B**). Therefore, RiLK1 and RiLK3 could also translocate across lipid bilayers as cell-penetrating peptide (CPP)-type.

These results supported the results obtained in a previous study, in which the Kd and Bmax values evidenced a better affinity of RiLK1 to the bacterial membranes than RiLK3 and tightly higher bound to *Salmonella* model membranes [**23**].

2.4. Dynamic light scattering and ζ-potential analysis

To evaluate the perturbation in specific membrane compositions, physical changes in our membrane mimetic systems promoted by RiLK1 were assessed by Dynamic Light Scattering (DLS) and ζ-potential measurements (**Fig. 7**). Firstly, the contribution of the electrostatic forces in peptide-biomembrane model interaction, was analysed in control tests by zeta-potential measurements on *Salmonella*- or *Staphylococcus*-like liposomes at 0.2 mM concentration without the addition of the peptide but in the presence of different concentrations of Ca^{2+}. The obtained results suggested a concentration-dependent trend for both the bacterial vesicles, which were completely shielded at the highest concentration of Ca^{2+} (passing from -70 ± 6 mV to -18 ± 4 mV for *Salmonella* and from -105 ± 10 mV to -28 ± 6 mV for *Staphylococcus*), leading to the neutralization of the negatively charged lipids (**Fig. 7C,F**). Moreover, DLS measurements did not reveal variations in size distribution of liposomes at all the Ca^{2+} concentrations tested, showing an average hydrodynamic diameter (*d*) of 500 ± 250 nm for *Salmonella* and different populations with mean sizes of 100 ± 20 nm (d1) and 900 ± 450 nm (d2) for *Staphylococcus,* with polydispersity indexes (PDI) of 0.3 (**Fig. 7B**) or 0.5, respectively (**Fig. 7E**). Therefore, it seems that the neutralization process was not sufficient to induce aggregation and/or fusion of liposomes investigated. Intriguingly, a different behaviour for the tested membrane mimetic systems was detected upon addition of RiLK1 at different concentrations ranging from 0.0025 to 0.1 mM. Specifically, DLS measurements at low peptide concentrations (below 0.010 mM) showed a homogeneous distribution of the *Salmonella* particle sizes with diameters corresponding to those of the liposomes alone (**Fig. 7A**), resulting only partially neutralized by RiLK1 (-65 ± 7 mV at 0.0025 mM and -37 ± 8 mV at 0.005 mM) (**Fig. 7C**). Conversely, at higher peptide concentrations (0.010 and 0.1 mM), where the ζ -potentials reached their maximal values (about -16 ± 6 mV at 0.01 mM and -12 ± 4 mV at 0.1 mM) (**Fig. 7C**), the bacterial vesicles distribution remained unimodal but characterized by a population of much larger sizes (d= 2300 ± 800 nm, PDI= 0.65 at 0.1 mM), indicating that RiLk1 promoted a cooperative and massive liposome aggregation, leading increased turbidity, flocculation and, finally, precipitation due to membrane disruption (**Fig. 7A**). Concerning *Staphylococcus,* again the interaction with RiLK1 at low concentrations (0.0025 and 0.005 mM) did not induce significant variations in the mean size, but only a broadening of the curve peaks due to the interaction of the peptides with the membranes (**Fig. 7D**). Differently from *Salmonella*-like liposomes, the solution became opalescent at 0.01 mM of RiLK1, thus

hindering the correct measurement of the hydrodynamic size (**Fig. 7D**). Flocculation of the membranes was observed after the interaction with RiLK1 at the highest concentration (0.1 mM) due to membrane disruption and aggregation, where the DLS size distribution was found to be 2500 ± 900 nm, and the PDI increased up to 0.8. These results were not in parallel with the ζ-potential values, showing that the strongly negative S*taphylococcus*-like membranes (-105 ± 10 mV) were not neutralized by RiLK1 at all the tested concentrations, reaching the maximum at 0.1 mM (-45 ± 5 mV) (**Fig. 7F**).

In the light of the analyses carried out, different mechanisms could be invoked to account for the mode of action of RiLK1 on bacterial liposomes. Specifically, our experimental conditions suggest a general CPP-internalization mechanism through multiple pathways for RiLK1 against S*taphylococcus*-like membranes although a bridging phenomenon among the liposomes could drive their aggregation observed at higher concentrations of RiLK1 (0.01 and 0.1 mM) following the peptide-peptide interactions. On the other hand, RiLK1 induces a permeabilization mechanism concerning *Salmonella*-like membranes above a threshold concentration as well as increased particle sizes. However, further studies will be necessary to investigate the mechanistic details undelight the antibacterial activity of our peptides.

2.5. Bacteriostatic activity of RILK1 and RILK3 against a MDR Enterococcus faecium

The human and animal microbiota are normally composed of numerous bacteria whose harmlessness/pathogenicity is strictly dependent on intestinal health. Enterococci are commensal bacteria and represent approximately 1% of microbiota **[34]**; among these, *Enterococcus faecium* (*E. faecium;* Efm) and *Enterococcus faecalis* (*E. faecalis*; Efs) are equally abundant in the gastrointestinal tract of healthy individuals **[35]**. Some authors have described their role as protector against invasions of pathogens **[36]**, however various intestinal imbalances can upset the organisation and transform these commensal bacteria into pathogenic bacteria **[37]**. Indeed, they have the potential to cause invasive infections thanks to their ability to both colonise surfaces and resist many antibiotics **[38]**. Efm and Efs are the most frequently isolated species in nosocomial settings **[39]**. Nonetheless, Efm is the most feared species due to its intrinsic or acquired resistance to many antibiotics which causes therapeutic failures in long-term hospitalised patients whose microbiota is dominated by it. Resistance to vancomycin (Vancomycin-Resistant Enterococci (VRE); VREfm strains) is widely reported, and its involvement in episodes of serious infections in hospital settings has alarmed the scientific community. The World Health Organization (WHO) has listed VREfm as a high-priority pathogen requiring timely research and drug development **[40]**. In this contest, antimicrobial peptides could represent potential candidates in the fight against these dangerous bacteria. To demonstrate this hypothesis, a strain of Efm, belonging to the Strains Collection of the Department of Veterinary Medicine and Animal Production of the University of Naples, was used to evaluate its susceptibility to both antibiotics and peptides.

In agreement with the scientific community and the surveillance report on "Antimicrobial resistance in the EU/EEA (EARS-Net)" for the year 2022 **[41]**, the strain of Efm was found to be resistant to vancomycin (R < 12 mm; EUCAST breakpoints). Furthermore, a high level of resistance has also been described against Ampicillin (R < 8 mm; EUCAST breakpoints), Ciprofloxacin (R < 15 mm; EUCAST breakpoints) and Levofloxacin (R < 15 mm; EUCAST breakpoints). These results are consistent with those of other authors. Specifically, Ayobami et al. **[42]** demonstrated that 99.4% of VREfm strains analysed exhibited co-resistance to

ampicillin. Resistance to antibiotics of the fluoroquinolones class (ciprofloxacin and levofloxacin) is not uncommon, and high-level ciprofloxacin resistance (HLCR) have been increasingly described **[43, 44]**. Fortunately, no resistance was found against Imipenem (50 mm; R < 21 mm; EUCAST breakpoints), Eravacycline (30 mm; R < 24 mm; EUCAST breakpoints) and Tigecycline (24 mm; R < 22 mm; EUCAST breakpoints). This last data was not obvious considering that resistance to this antibiotic, considered among those with the highest therapeutic efficacy, is increasing [**45]**. Overall, since bacteria resistant to at least three classes of antibiotics have been defined as Multidrug-Resistant (MDR), the Efm strain can be considered MDR-bacterium and its use in susceptibility testing against RiLK1 and RiLK3 peptides makes the experiment challenging.

E. faecium strain showed a high sensitivity towards both peptides, even at the lowest concentrations tested (**Table 3**). Although differences have been found concerning the peptide used and the starting inoculum concentration, the MIC values recorded were never higher than 2.5 μM. Interestingly, an almost negligible difference was found between the MIC values obtained with inoculum at different concentrations (differences less than 1 μM). However, there seems to be a correlation between peptide dose (μM) and bacterial load (Log (cfu/mL)) which could be expressed as ~0.6 for RiLK1 and ~0.4 for RiLK3 (mean of MIC values/Log (cfu/mL) of starting inoculum); it means that for each bacterial Log (cfu/mL), 0.55 μM or 0. 35 μM of RiLK1 and RiLK3, respectively, would seem necessary to inhibit replication.

In more detail, the "daughter" peptide, developed from the RiLK1 sequence, showed greater bacteriostatic efficacy. Looking at the graphs in **Fig. 8**, it is possible to see how bacterial replication was interrupted when the Efm strain was treated with the RiLK3 peptide at the concentration of the MIC values; the bacterial load after incubation was the same as the starting inoculum.

Both peptides showed bacteriostatic action at very small doses, suggesting their use in combined treatments with a low-dose antibiotic of choice. Aware of the negative effects of the improper use (high doses and/or long-term treatment) of antibiotics on the development of resistance phenomena, their combined use with natural molecules with high bacteriostatic efficiency could allow the treatment doses to be reduced and, therefore, contain the development of resistance phenomena. Several authors have recently demonstrated the potential synergistic or additive effects of a drug cocktail, composed of antimicrobial peptides and antibiotics **[8, 46]**. By combining AMPs and antibiotics, both additive and synergistic effects on MDR isolates make it possible to achieve important objectives such as the use of antibiotics currently set aside due to therapeutic failures resulting from their use. In fact, by adding AMPs to antibiotics it is possible to make these antibiotics effective, even if used in the same doses **[46]**. As previously mentioned, VREfm bacteria constitute a serious public health concern and alternative treatment protocols must be developed. Further studies will thoroughly investigate the effect of adding RiLK1 and RiLK3 to common antibiotics used to treat infections caused by VREfm bacteria.

3. Conclusions

The interaction of the lytic peptides with model membranes is an important way to understand the physicochemical bases of the mechanism and selectivity of this class of molecules. So far, several different modes of action have been predicted for antimicrobial peptides, but their

partition to the water-lipid bilayer interface is common to all these compounds [**33**]. However, despite extensive studies, the mode of action of these antimicrobials is not fully understood and the basis for their selectivity towards specific target cells has been only partially clarified.

In our previous work, the peptide RiLK3 was designed by substituting a Lys residue in the parental decapeptide RiLK1 with Arg, to investigate the effects of this modification on the structural properties and antimicrobial activity. Indeed, the relationship between chemico-physical features and biological functions of AMPs is often nonlinear as small changes in peptide structure can lead to disproportionate effects on activity and toxicity, complicating the establishment of straightforward correlations, which remain elusive due to the complex and multifaceted nature of these antimicrobials.

In the current study, fluorescence spectroscopy and Dynamic Light Scattering was used to obtain further information about the interaction of these compounds with the bacterial lipid bilayer.

It has been reported that the mechanism of action of AMPs involves two stages, initial electrostatic interaction of the cationic residues of the peptides with the anionic lipids of the bacterial membrane [**47,48**] followed by hydrophobic interaction of the aromatic side chains of amino acids with the lipid bilayer, that is crucial for membrane disruption [**49-51**]. Consistent with this behaviour, fluorescence assays (blue shifts, fluorescence quenching by water-soluble and membrane-embedded quenchers) and K_{SV} values demonstrated that RiLK1 and RiLK3 interact tightly with liposomes mimicked the membranes of *S.* Typhimurium or *S. aureus*, locating close to the lipid/water interface region. Moreover, peptide-induced liposome leakage was observed, suggesting that RiLK1 and RiLK3 can cause instability of membranes at high concentrations inducing a transient increase of membrane permeation by altering the fluidity properties of lipid bilayers and showing no formation of stable pores. However, both peptides could also behave as CPP-like against *Staphylococcus* liposomes at concentrations near to their MIC values without causing membrane damage. Most importantly, both molecules were found to show potent bacteriostatic efficacy against MDR-resistant *E. faecium* strain, suggesting that RiLK1 and RiLK3 can be used in combination with known antibiotics in the treatment of infections caused by VREfm bacteria offering a new approach to combat antibiotic resistance.

4. Methods

4.1. Synthesis of peptides

Both antimicrobial peptides RiLK1 (RLKWVRIWRR-NH_2) and RiLK3 (RLRWVRIWRR-NH_2) were purchased from GenScript Biotech (Leiden, Netherlands) at >95% purity. They were stored as a lyophilized powder at -20 °C. Analysis by mass spectrometry confirmed the identity of peptides.

4.2. Preparation of multilamellar vesicles

Journal Pre-proofs

Model lipid membranes (liposomes) were prepared as reported in Agrillo et al [**23**].

4.3. Fluorescence Spectroscopy studies

Fluorescence measurements were carried out with a Shimadzu RF-6000 spectrofluorometer (Kyoto, Japan), at 25 °C using a 1-cm path-length quartz cell (Hellma Analytics, Milan, Italy).

Trp emission fluorescence spectra were recorded from 300 to 500 nm using a 280 nm excitation wavelength, setting the slit widths at 5 nm. Each fluorescence spectrum of peptide was corrected by subtracting the baseline for the same concentration of lipid vesicles in buffer solution.

For the blue-shift fluorescence spectroscopy studies, peptide solutions (20 μM) in 10 mM HEPES (Sigma-Aldrich) containing 100 mM NaCl (Sigma-Aldrich), pH 7.2, were incubated for 30 min at 25 °C in the absence or presence of increasing concentrations of lipid vesicles (ranging from 0 to 2 mM).

4.4. Fluorescence Quenching of Trp Emission by Water-soluble and Lipophilic Probes

Acrylamide quenching assays were conducted *via* addition of increasing concentrations of the water-soluble quencher acrylamide (from 0 to 200 mM). A 4.0-M stock solution of acrylamide was prepared in 10 mM HEPES (Sigma-Aldrich) and NaCl 100 mM (Sigma-Aldrich), pH 7.2. Aliquots of this solution were added to 1.0 μM solution of Trp-containing peptides in the absence and presence of 30 μM lipid vesicles at 25 °C after 30 min incubation. To reduce absorbance by acrylamide, excitation of tryptophan at 295 nm instead of 280 nm was used. The effect of the quencher on the fluorescence of each peptide was analysed according to the Stern–Volmer equation,

$$F0/F=1+Ksv\,[Q] \qquad (1)$$

where F0 and F represent the fluorescence intensities in the absence or presence of the quencher (Q), respectively, Ksv is the Stern–Volmer quenching constant, which is a measure of the accessibility of Trp to acrylamide, and [Q] is the concentration of the quencher.

Quenching studies with lipophilic probes 5-NS or 16-NS were conducted by adding increasing concentrations of the quenchers (from 2.5 to 40 μM). 100 mM-stock solutions of the lipophilic probes were prepared in ethanol. Small aliquots of these solutions were added to the samples of 2 μM peptide incubated with 60 μM lipid vesicles in 50 mM Tris-HCl containing 50 mM NaCl, pH 7.2, after 30 min incubation. The final ethanol concentration was kept below 2% (v/v) to avoid lipid bilayer perturbations [**52**]. The fluorescence quenching data were analysed according to the Stern-Volmer equation. All experiments were performed in triplicate and the Ksv values were calculated from the slopes of the plots obtained by linear regression analysis.

4.5. Lipid vesicle leakage assays

Perturbation of membrane permeability was determined by measuring the release of a fluorophore 5-Carboxyfluorescein (CF) (Sigma-Aldrich) entrapped inside large unilamellar vesicles (LUVs). Lipid films were prepared as described as above for a final concentration of 5 mM. After being dried under vacuum at least for 3 h, the lipids were hydrated with 10 mM HEPES and 100 mM NaCl, pH 7.2, containing 25 mM CF by vigorous vortexing. At this concentration, the fluorescence of CF was self-quenched. The suspension was extruded through polycarbonate filters (1 µm pore-size filters, 11 times) by a mini-extruder (Avanti Polar Lipids Inc., Alabaster, AL, USA) to create LUVs. Free CF was removed by gel filtration chromatography, passing the extruded LUVs through a Superdex 30 Increase 10/300 GL column (GE Healthcare, Milan, Italy) connected to an AKTA FPLC system (GE Healthcare, Milan, Italy) eluted with 10 mM HEPES, pH 7.2, containing 100 mM NaCl. Liposomes containing entrapped CF were incubated with RiLK1 or RiLK3 at 15 µM and 30 µM concentration in 10 mM HEPES, pH 7.2, containing 100 mM NaCl at 20 °C for 30 min. The fluorescence intensity of the CF released from the liposomes was recorded at 25 °C every 3 min until 30 min using an excitation wavelength of 490 nm and an emission wavelength ranging from 500 to 600 nm. At the end of each experiment, the maximum fluorescence intensity corresponding to 100% leakage was determined by the addition of the detergent Triton X-100 (0.25 %) to the sample.

The percentage of CF leakage caused by the peptide was calculated in accordance with the following equation,

$$\% \text{ CF leakage} = (Ft\text{-}Fi) \times 100 / (Fd\text{-}Fi) \qquad (2)$$

where Ft and Fi are the fluorescence intensities in the presence and absence of peptides, respectively, before the addition of Triton X-100, and Fd is the fluorescence measured after disruption with Triton X-100. All experiments were performed in triplicate.

.

4.6. Antibacterial susceptibility testing to antibiotics

Antimicrobial susceptibility testing of *Enterococcus faecium* was performed using the disk diffusion method following the recommendations of the European Committee for Antimicrobial Susceptibility Testing (EUCAST, 2024). The antimicrobials used were ampicillin (2 µg), vancomycin (5 µg), ciprofloxacin (5 µg), levofloxacin (5 µg), imipenem (10 µg), eravacycline (20 µg), and tigecycline (15 µg). The inhibition zones were measured and the results were interpreted in accordance with the EUCAST breakpoints specific for *Enterococcus* spp. Thereby, *E. faecium* isolates were classified as resistant (R) and sensitive (S), according to EUCAST breakpoints, and as MDR using the criteria of Magiorakos et al. **[54]**.

Journal Pre-proofs

4.7. Antimicrobial susceptibility testing to AMPs: Minimum inhibitory concentration (MIC)

The AMP susceptibility assay was carried out using the broth microdilution method in 96-well microplates, according to the guidelines of the European Committee for Antimicrobial Susceptibility Testing (EUCAST, 2024) **[55]** and ISO 20776-1.

The method was based on the preparation of working solutions of antimicrobial agents, in volumes of 100 µl per well (with the addition of a maximum of 10 µl inoculum volume). At least one well, containing 100 µl of medium free of antimicrobial agents, must be included as a growth control for each strain tested. Similarly, a well containing 100 µl of medium free of antimicrobial agents should be included as an uninoculated negative control well for each organism tested.

Bacterial inoculum was prepared by revitalizing the strains in 10 mL of Muller Hilton Broth (MHB, Oxoid Ltd, Wade Road, Basingstoke, Hants, RG24 8PW, UK), incubated for 18±2 h at 37°C, until a turbidity equal to or greater than 0.5 McFarland, which correspond to 1×10^8 cfu/mL; if necessary, the culture was adjusted. The final concentration of inoculum tested was of 5×10^5 cfu/mL (target range, 2×10^5 cfu/mL to 8×10^5 cfu/mL), in agreement with EUCAST guidelines **[55]**. Furthermore, experiments were also conducted with inoculum of 5×10^3 cfu/mL. Each strain was exposed to different concentrations of RiLK1 and RiLK3. The peptide stock solutions (5mM) were obtained by dissolving them in distilled water; meanwhile, the intermediate peptide solutions were produced daily by sonicating the frozen stock solution and diluting it with MHB. Briefly, each well of the microplate was filled with 10 µL of bacterial suspension (5×10^5 cfu/mL or 5×10^3 cfu/mL) and 90 µL of peptide solutions at decreasing concentrations from 140 µM to 1 µM. Then, the microplates were incubated at 37 °C for 18±2 hours. The MIC was defined as the lowest concentration of an antimicrobial agent at which no growth was detected. Furthermore, viable bacterial counts were determined.

4.8. Morphological characterization and surface charge measurements

The hydrodynamic size and ζ-potential of *Salmonella*-like or *Staphylococcus*-like liposomes were measured by Zetasizer Nano-ZS instrument (Malvern Instrument Ltd., Cambridge, United Kingdom) equipped with a He–Ne laser (633 nm, fixed scattering angle of 173°, 25°C). The size (*d*) and the polydispersity index (PDI) of the obtained liposomes (at an initial concentration of 2 mM) were measured by diluting them down to 0.2 mM in MilliQ water. The liposome suspensions (1 mL) were inserted in a standard disposable cuvette and three measurements ($n = 3$) of their size and PDI were performed. The hydrodynamic size measurements were performed after 30 min interaction with RiLK1 peptide at different concentrations (0.0025, 0.005, 0.01, 0.1 mM). The ζ-potential of the bacterial-mimic liposomes and the peptides (before and after their interaction with them) was measured in triplicate (n=3) by using disposable zeta-potential cuvettes (1 mL). ζ-potential measurements were performed for liposome:peptide interaction monitoring in suspensions of *Salmonella*-like or *Staphylococcus*-like liposomes with RiLK1 (0.0025, 0.005, 0.01, 0.1 mM mM). Analogously, a control with $CaCl_2$ was performed by measuring DLS and ζ -potential before and after incubations with 0.1, 1.0, and 4.5 mM concentrations.

4.9. Statistical Analyses

Statistical analyses were performed using GraphPad Prism®, version 8.0.1 (GraphPad, San Diego, CA, USA). All experiments were performed at least three times, and the data were presented as the mean (M) ± standard error (SE). GraphPad Prism® was used to assess the data from the fluorescence assays (blue shift, quenching and leakage assays).

CRediT authorship contribution statement

Lorena Gratino: Investigation, Methodology. Marta Gogliettino: Conceptualization, Formal analysis, Writing – original draft, Writing – review & editing. Marco Balestrieri: Conceptualization, Software, Visualization. Alessandra Porritiello: Investigation, Methodology. Principia Dardano: Investigation, Visualization. Bruno Miranda: Investigation, Methodology. Monica Ambrosio: Investigation, Methodology, Visualization. Rosa Luisa Ambrosio: Investigation, Validation. Luigi Nicolais: Funding Acquisition, Supervision. Gianna Palmieri: Conceptualization, Funding Acquisition, Supervision, Writing – review & editing.

Declaration of competing interest

The authors declare that they have no known competing financial interests or personal relationships that could have appeared to influence the work reported in this paper.

Data availability

Data will be made available on request.

Acknowledgments

This work was financially supported by the Ministry of Health-project APACHE- Ricerca Corrente 2022 IZS 10/22 RC; Ministry of University and Research- project NUTRAGE FOE-2021 DBA.AD005.225.

Appendix A. Supplementary data

Supplementary data to this article can be found online at

Journal Pre-proofs

Journal Pre-proofs

References

1. J. Wang, X. Dou, J. Song, Y. Lyu, X. Zhu, L. Xu, L. Weizhong, A. Shan, Antimicrobial peptides: promising alternatives in the post feeding antibiotic era, Med. Res. Rev. 39(3) (2019) 831–859. https://doi.org/10.1002/med.21542.

2. M. Pasupuleti, A. Schmidtchen, M. Malmsten, Antimicrobial peptides: key components of the innate immune system, Crit. Rev. Biotechnol. 32(2) (2012) 143-171. https://doi.org/10.3109/07388551.2011.594423.

3. I. Mohammed, D.G. Said, H.S. Dua, Human antimicrobial peptides in ocular surface defense, Prog. Retin Eye Res. 61 (2017) 1–22. https://doi.org/10.1016/j.preteyeres.2017.03.004.

4. H.K. Kang, C. Kim, C.H. Seo, Y. Park, The therapeutic applications of antimicrobial peptides (AMPs): a patent review, J. Microbiol. 55(1) (2017) 1–12. https://doi.org/10.1007/s12275-017-6452-1.

5. J. Lei, L. Sun, S. Huang, C. Zhu, P. Li, J. He, V. Mackey, D.H. Coy, Q. He, The antimicrobial peptides and their potential clinical applications, Am. J. Transl. Res. 11(7) (2019) 3919–3931.

6. E.H.M. Mohammed, S. Lohan, T. Ghaffari, S. Gupta, R.K. Tiwari, K. Parang, Membrane-Active Cyclic Amphiphilic Peptides: Broad-Spectrum Antibacterial Activity Alone and in Combination with Antibiotics, J. Med. Chem. 65(23) (2022) 15819-15839. https://doi.org/10.1021/acs.jmedchem.2c01469.

7. C. Bucataru, C. Ciobanasu, Antimicrobial peptides: Opportunities and challenges in overcoming resistance, Microbiol. Res. 286 (2024) 127822. https://doi.org/10.1016/j.micres.2024.127822.

8. Y. Zhu, W. Hao, X. Wang, J. Ouyang, X. Deng, H. Yu, Y. Wang, Antimicrobial peptides, conventional antibiotics, and their synergistic utility for the treatment of drug-resistant infections, Med. Res. Rev. 42(4) (2022) 1377-1422. https://doi.org/10.1002/med.21879.

9. A.H. Benfield, S.T. Henriques, Mode-of-Action of Antimicrobial Peptides: Membrane Disruption vs. Intracellular Mechanisms, Front. Med. Technol. 2 (2020) 610997. https://doi.org/10.3389/fmedt.2020.610997

10. T. Singh, P. Choudhary, S. Singh, Antimicrobial Peptides: Mechanism of Action. Insights on Antimicrobial Peptides, IntechOpen (2022). http://dx.doi.org/10.5772/intechopen.99190.

11. H. Sato, J.B. Feix, Peptide-membrane interactions and mechanisms of membrane destruction by amphipathic alpha-helical antimicrobial peptides. Biochim. Biophys. Acta 1758(9) (2006) 1245-1256. https://doi.org/10.1016/j.bbamem.2006.02.021.

12. S.R. Dennison, L.H. Morton, F. Harris, D.A. Phoenix, The impact of membrane lipid composition on antimicrobial function of an alpha-helical peptide, Chem. Phys. Lipids. 151(2) (2008) 92-102. https://doi.org/10.1016/j.chemphyslip.2007.10.007.

13. D. Roversi, C. Troiano, E. Salnikov, L. Giordano, F. Riccitelli, M. De Zotti, B. Casciaro, M.R. Loffredo, Y. Park, F. Formaggio, M.L. Mangoni, B. Bechinger, L. Stella, Effects of antimicrobial peptides on membrane dynamics: A comparison of fluorescence and NMR experiments, Biophys. Chem. 300 (2023) 107060. https://doi.org/10.1016/j.bpc.2023.107060.

14. G. Bocchinfuso, A. Palleschi, B. Orioni, G. Grande, F. Formaggio, C. Toniolo, Y. Park, K.S. Hahm, L. Stella, Different mechanisms of action of antimicrobial peptides: insights from fluorescence spectroscopy experiments and molecular dynamics simulations, J. Pept. Sci. 15 (2009) 550–558. https://doi.org/10.1002/psc.1144.

15. K. Matsuzaki (Ed.), Antimicrobial Peptides: Basics for Clinical Application, Springer, Singapore, 2019. https://doi.org/10.1007/978-981-13-3588-4.

Journal Pre-proofs

16. J. Knobloch, D.K. Suhendro, J.L. Zieleniecki, J.G. Shapter, I. Koper, Membrane-drug interactions studied using model membrane systems, Saudi J. Biol. Sci. 22 (2015) 714–718. https://doi.org/10.1016/j.sjbs.2015.03.007.

17. A. Hollmann, M. Martinez, P. Maturana, L.C. Semorile, P.C. Maffia, Antimicrobial peptides: interaction with model and biological membranes and synergism with chemical antibiotics, Front. Chem. 6 (2018) 204. https://doi.org/10.3389/fchem.2018.00204.

18. G. Palmieri, M. Balestrieri, F. Capuano, Y.T.R. Proroga, F. Pomilio, P. Centorame, A. Riccio, R. Marrone, A. Anastasio, Bactericidal and antibiofilm activity of bactenecin-derivative peptides against the food-pathogen Listeria monocytogenes: New perspectives for food processing industry, Int. J. Food Microbiol. 279 (2018) 33-42. https://doi.org/10.1016/j.ijfoodmicro.2018.04.039Get rights and content.

19. A. Colagiorgi, R. Festa, P.A. Di Ciccio, M. Gogliettino, M. Balestrieri, G. Palmieri, A. Anastasio, A. Ianieri, Rapid biofilm eradication of the antimicrobial peptide 1018-K6 against *Staphylococcus aureus*: a new potential tool to fight bacterial biofilms, Food Control 197 (2020) 106815. https://doi.org/10.1016/j.foodcont.2019.106815.

20. R. Hancock, H.G. Sahl, Antimicrobial and host-defense peptides as new anti-infective therapeutic strategies, Nat. Biotechnol. 24 (2006) 1551–1557. https://doi.org/10.1038/nbt1267.

21. B. Agrillo, Y.T.R. Proroga, M. Gogliettino, M. Balestrieri, R. Tatè, L. Nicolais, G. Palmieri, A Safe and Multitasking Antimicrobial Decapeptide: The Road from De Novo Design to Structural and Functional Characterization, Int. J. Mol. Sci. 21(18) (2020) 6952. https://doi.org/10.3390/ijms21186952.

22. L. Falcigno, G. D'Auria, G. Palmieri, M. Gogliettino, B. Agrillo, R. Tatè, P. Dardano, L. Nicolais, M. Balestrieri, Key Physicochemical Determinants in the Antimicrobial Peptide RiLK1 Promote Amphipathic Structures, Int. J. Mol. Sci. 22(18) (2021) 10011. https://doi.org/10.3390/ijms221810011.

23. B. Agrillo, A. Porritiello, L. Gratino, M. Balestrieri, Y.T. Proroga, A. Mancusi, L. Cozzi, T. Vicenza, P. Dardano, B. Miranda, P.V. Escribá, M. Gogliettino, G. Palmieri, Antimicrobial activity, membrane interaction and structural features of short arginine-rich antimicrobial peptides, Front. Microbiol. 14 (2023) 1244325. https://doi.org/10.3389/fmicb.2023.1244325.

24. L.W. Hamoen, M. Wenzel, Antimicrobial peptides-interaction with membrane lipids and proteins, Front. Cell Dev. Biol. 5 (2007) 1–3. https://doi.org/10.3389/fcell.2017.00004.

25. W.C. Wimley, Describing the mechanism of antimicrobial peptide action with the interfacial activity model, ACS Chem. Biol. 5 (2010) 905–917. https://doi.org/10.1021/cb1001558.

26. A.B.T. Ghisaidoobe, S.J. Chung, Intrinsic Tryptophan Fluorescence in the Detection and Analysis of Proteins: A Focus on Förster Resonance Energy Transfer Techniques, Int. J. Mol. Sci. 15 (2014) 22518-22538. https://doi.org/10.3390/ijms151222518.

27. G.F. Ames, Lipids of Salmonella typhimurium and Escherichia coli: structure and metabolism, J. Bacteriol. 95(3) (1968) 833-143. https://doi.org/10.1128/JB.95.3.833-843.1968.

Journal Pre-proofs

28. S.C. Barbosa, T.M. Nobre, D. Volpati, E.M. Cilli, D.S. Correa, O.N. Jr. Oliveira, The cyclic peptide labaditin does not alter the outer membrane integrity of Salmonella enterica serovar Typhimurium, Sci. Rep. 9(1) (2019) 1993. https://doi.org/10.1038/s41598-019-38551-5.

29. P.R. Beining, E. Huff, B. Prescott, T.S. Theodore, Characterization of the lipids of mesosomal vesicles and plasma membranes from Staphylococcus aureus, J. Bacteriol. 121(1) (1975) 137-143. https://doi.org/10.1128/jb.121.1.137-143.1975.

30. D.C. White, F.E. Frerman, Extraction, characterization, and cellular localization of the lipids of Staphylococcus aureus, J. Bacteriol. 94(6) (1967) 1854-1867. https://doi.org/10.1128/jb.94.6.1854-1867.1967.

31. F. Moro, F.M. Goñi, M.A. Urbaneja, Fluorescence quenching at interfaces and the permeation of acrylamide and iodide across phospholipid bilayers, FEBS Lett. 330 (1993) 129–132. https://doi.org/10.1016/0014-5793(93)80257-U.

32. A.J. Pérez-Berná, J. Guillén, M.R. Moreno, A. Bernabeu, G. Pabst, P. Laggner, J. Villalaín, Identification of the membrane-active regions of hepatitis C virus p7 protein: biophysical characterization of the loop region, J. Biol. Chem. 283(13) (2008) 8089-8101. https://doi.org/10.1074/jbc.M709413200.

33. W.C. Wimley, K. Hristova, The Mechanism of Membrane Permeabilization by Peptides: Still an Enigma, Aust. J. Chem. 73 (2020) 96. https://doi.org/10.1071/CH19449.

34. K. Korpela, E.W. Blakstad, S.J. Moltu, K. Strømmen, B. Nakstad, A.E. Rønnestad, K. Brække, P.O. Iversen, C.A. Drevon, W. de Vos, Intestinal microbiota development and gestational age in preterm neonates, Sci. Rep. 8 (2018) 1-9. http://dx.doi.org/10.1038/s41598-018-20827-x.

35. F. Lebreton, A.L. Manson, J.T. Saavedra, T.J. Straub, A.M. Earl, M.S. Gilmore, Tracing the enterococci from Paleozoic origins to the hospital, Cell 169 (2017) 849–861.e13. https://doi.org/10.1016/j.cell.2017.04.027.

36. S. Arredondo-Alonso, J. Top, A. McNally, S. Puranen, M. Pesonen, J. Pensar, P. Marttinen, J.C. Braat, M.R.C. Rogers, W. van Schaik, S. Kaski, R.J.L. Willems, J. Corander, A.C. Schürch, Plasmids shaped the recent emergence of the major nosocomial pathogen Enterococcus faecium, mBio 11 (2020) e03284-19. https://doi.org/10.1128/mbio.03284-19.

37. F. Lebreton, W. van Schaik, A. M. McGuire, P. Godfrey, A. Griggs, V. Mazumdar, J. Corander, L. Cheng, S. Saif, S. Young, Q. Zeng, J. Wortman, B. Birren, R.J. Willems, A.M. Earl, M.S. Gilmore, Emergence of epidemic multidrug-resistant Enterococcus faecium from animal and commensal strains. mBio. 4(4) (2013) e00534-13. https://doi.org/10.1128/mbio.00534-13.

38. A.R. Freitas, A.P. Pereira, C. Novais, L. Peixe, Multidrug-resistant high-risk Enterococcus faecium clones: can we really define them? Int. J. Antimicrob. Agents. 57(1) (2021) 106227. https://doi.org/10.1016/j.ijantimicag.2020.106227.

39. Y. Zhang, M. Du, Y. Chang, C. Liang-an, Q. Zhang, Incidence, clinical characteristics, and outcomes of nosocomial Enterococcus spp. bloodstream infections in a tertiary-care hospital in Beijing, China: a four-year retrospective study, Antimicrob. Resist. Infect. Control 6(1) (2017) 73. https://doi.org/10.1186/s13756-017-0231-y.

Journal Pre-proofs

40. E. Tacconelli, E. Carrara, A. Savoldi, S. Harbarth, M. Mendelson, D.L. Monnet, C. Pulcini, G. Kahlmeter, J. Kluytmans, Y. Carmeli, M. Ouellette, K. Outterson, J. Patel, M. Cavaleri, E.M. Cox, C.R. Houchens, M.L. Grayson, P. Hansen, N. Singh, U. Theuretzbacher, N. Magrini, WHO Pathogens Priority List Working Group, Discovery, research, and development of new antibiotics: the WHO priority list of antibiotic-resistant bacteria and tuberculosis, Lancet Infect. Dis. 18(3) (2018) 318–327. https://doi.org/10.1016/S1473-3099(17)30753-3.

41. European Centre for Disease Prevention and Control. Antimicrobial resistance in the EU/EEA (EARS-Net) - Annual Epidemiological Report 2022. Stockholm: ECDC; 2023.

42. O. Ayobami, N. Willrich, A. Reuss, T. Eckmanns, R. Markwart, The ongoing challenge of vancomycin-resistant Enterococcus faecium and Enterococcus faecalis in Europe: an epidemiological analysis of bloodstream infections, Emerg. Microbes & Infect. 9(1) (2020) 1180-1193. https://doi.org/10.1080/22221751.2020.1769500.

43. M.O. Ahmed, and K.E. Baptiste, Vancomycin-resistant enterococci: a review of antimicrobial resistance mechanisms and perspectives of human and animal health, Microb. Drug Resist. 24 (2018) 590–606. https://doi.org/10.1089/mdr.2017.0147.

44. L.D.R. dos Santos, J.P.R. Furlan, I.F.L. Gallo, M.S. Ramos, E.A. Savazzi, E.G. Stehling, Occurrence of multidrug-resistant Enterococcus faecium isolated from environmental samples, Lett. Appl. Microbiol. 73 (2) (2021) 237–246, https://doi.org/10.1111/lam.13508.

45. M. Dadashi, P. Sharifian, N. Bostanshirin, B. Hajikhani, N. Bostanghadiri, N. Khosravi-Dehaghi, D. Darban-Sarokhalil, The global prevalence of daptomycin, tigecycline, and linezolid-resistant Enterococcus faecalis and Enterococcus faecium strains from human clinical samples: a systematic review and meta-analysis, Front. Med. 8 (2021) 720647. https://doi.org/10.3389/fmed.2021.720647

46. A. Jahangiri, A. Neshani, S. A. Mirhosseini, K. Ghazvini, H. Zare, H. Sedighian, Synergistic effect of two antimicrobial peptides, Nisin and P10 with conventional antibiotics against extensively drug-resistant Acinetobacter baumannii and colistin-resistant Pseudomonas aeruginosa isolates, Microb. Pathog.150 (2021) 104700. https://doi.org/10.1016/j.micpath.2020.104700.

47. A.H. Juffer, C.M. Shepherd, H.J. Vogel, Protein-membrane electrostatic interactions: applications of the Lekner summation technique, J. Chem. Phys. 114 (2001) 1892–1905. https://doi.org/10.1063/1.1334901.

48. C.M. Shepherd, K. A. Schaus, H. J. Vogel, A.H. Juffer, Molecular dynamics study of peptide-bilayer adsorption, Biophys. J. 80 (2001) 579–596. https://doi.org/10.1016/S0006-3495(01)76039-0.

49. T. Kiyota, S. Lee, G. Sugihara, Design and synthesis of amphiphilic a-helical model peptides with systematically varied hydrophobic-hydrophilic balance and their interaction with lipid and bio-membranes, Biochem. 35 (1996) 13196–13204. https://doi.org/10.1021/bi961289t.

50. O. Lequin, A. Ladram, L. Chabbert, F. Bruston, O. Convert, D. Vanhoye, G. Chassaing, P. Nicolas, M. Amiche, Dermaseptin S9, an alpha-helical antimicrobial peptide with a hydrophobic core and cationic termini. Biochem. 45(2) (2006) 468-480. https://doi.org/10.1021/bi051711i.

51. K.A. Henzler-Wildman, G.V. Martinez, M.F. Brown, A. Ramamoorthy, Perturbation of the hydrophobic core of lipid bilayers by the human antimicrobial peptide LL-37, Biochem 43 (2004) 8459–8469. https://doi.org/10.1021/bi036284s.

52. D.E. Chalpin, A.M. Kleinfeld, Interaction of fluorescence quenchers with the n-(9-anthroyloxy) fatty acid membrane probes, Biochim. Biophys. Acta 731 (1983) 465–474. https://doi.org/10.1016/0005-2736(83)90042-1.

53. M. Siepi, G. Donadio, P. Dardano, L. De Stefano, D.M. Monti, E. Notomista, Denatured lysozyme-coated carbon nanotubes: a versatile biohybrid material, Sci. Rep. 9(1) (2019) 16643. https://doi.org/10.1038/s41598-019-52701-9.

54. A.P. Magiorakos, A. Srinivasan, R.B. Carey, Y. Carmeli, M.E. Falagas, C.G. Giske, S. Harbarth, J.F. Hindler, G. Kahlmeter, B. Olsson-Liljequist, D.L. Paterson, L.B. Rice, J. Stelling, M.J. Struelens, A. Vatopoulos, J.T. Weber, D.L. Monnet, Multidrug-resistant, extensively drug-resistant and pandrug-resistant bacteria: An international expert proposal for interim standard definitions for acquired resistance, Clin. Microbiol. Infect. 18 (2012) 268–281. https://doi.org/10.1111/j.1469-0691.2011.03570.x

55. The European Committee on Antimicrobial Susceptibility Testing. Breakpoint tables for interpretation of MICs and zone diameters. Version 14.0, (2024). http://www.eucast.org.n.d.

Journal Pre-proofs

Figure Legends

Fig. 1. Changes in Trp fluorescence emission spectra upon the interaction of RiLK1 with MLVs. Fluorescence emission spectra of RiLK1 in the absence (buffer) and presence of increasing concentrations of (**A**) *S. aureus* (CL_{42}:$POPG_{58}$), (**B**) *S.* Typhimurium ($DOPE_{78}$:$POPG_{18}$:CL_4), (**C**) zwitterionic (PC) and (**D**) Eukaryotic (PC_{40}:$POPE_{40}$:SM_{15}:PS_5) multilamellar vesicles (MLVs) obtained upon excitation at 280 nm. (**E**) Blue shifts of tryptophan fluorescence emission determined as the difference among the wavelengths at the maximum emission in the absence and presence of lipids ($\Delta\lambda_{max} = \lambda_0 - \lambda$) plotted as a function of lipid concentration. Measurements were performed in 10 mM HEPES, 100 mM NaCl pH 7.2

at 25 °C, using a peptide concentration of 20 μM. All data are presented as the mean (M) ± standard deviation (SD).

Fig. 2. Changes in Trp fluorescence emission spectra upon the interaction of RiLK3 with MLVs. Fluorescence emission spectra of RiLK3 in the absence (buffer) and presence of increasing concentrations of (**A**) *S. aureus* (CL_{42}:$POPG_{58}$), (**B**) *S.* Typhimurium ($DOPE_{78}$:$POPG_{18}$:CL_4), (**C**) zwitterionic (PC) and (**D**) Eukaryotic (PC_{40}:$POPE_{40}$:SM_{15}:PS_5) multilamellar vesicles (MLVs) obtained upon excitation at 280 nm. E) Blue shifts of tryptophan fluorescence emission determined as the difference among the wavelengths at the maximum emission in the absence and presence of lipids ($\Delta\lambda_{max} = \lambda_0 - \lambda$) plotted as a function of lipid concentration. Measurements were performed in 10 mM HEPES, 100 mM NaCl pH 7.2, using a peptide concentration of 20 μM. All data are presented as the mean (M) ± standard deviation (SD).

Fig. 3. Acrylamide quenching and Ksv determination. (A) Stern-Volmer plots for the quenching of the Trp fluorescence emission of RiLK1 by acrylamide (Q) in aqueous buffer and in the presence of differently charged multilamellar vesicles. (**B**) Stern-Volmer plots for the quenching of the Trp fluorescence emission of RiLK3 by acrylamide in buffer and in the presence of differently charged multilamellar vesicles. 1.0 μM of RiLK1 and RiLK3 wasincubated in the absence and presence of 30 μM lipid vesicles. The spectra were acquired after 30 minutes of peptide-MLVs incubation. Experimental data was fitted to the Stern-Volmer equation.

Fig. 4. Emission fluorescence quenching by 16-NS e 5-NS of RiLK1 in bacterial MLVs. Tryptophan fluorescence emission spectra of RiLK1 with increasing concentrations of 16-NS (2.5-40 μM) in the presence of (**A**) *S.* Typhimurium ($DOPE_{78}$:$POPG_{18}$:CL_4), or (**B**) S. *aureus* (CL_{42}:$POPG_{58}$). Tryptophan fluorescence emission spectra of RiLK1 with increasing concentrations of 5-NS (2.5-40 μM) in the presence of (**C**) *S.* Typhimurium ($DOPE_{78}$:$POPG_{18}$:CL_4) or (**D**) S. *aureus* (CL_{42}:$POPG_{58}$). Stern-Volmer plots of the quenching of the Trp fluorescence emission of RiLK1 by 5-NS and 16-NS in (**E**) *S.* Typhimurium or (**F**) *S. aureus* MLVs. Q: quencher

Fig. 5. Emission fluorescence quenching by 16-NS e 5-NS of RiLK3 in bacterial MLVs. Tryptophan fluorescence emission spectra of RiLK3 with increasing concentrations of 16-NS (2.5-40 μM) in the presence of (**A**) *S.* Typhimurium ($DOPE_{78}$:$POPG_{18}$:CL_4), or (**B**) S. *aureus* (CL_{42}:$POPG_{58}$). Tryptophan fluorescence emission spectra of RiLK3 with increasing concentrations of 5-NS (20-100 μM) in the presence of (**C**) *S.* Typhimurium ($DOPE_{78}$:$POPG_{18}$:CL_4), or (**D**) S. *aureus* (CL_{42}:$POPG_{58}$). Stern-Volmer plots of the quenching of the Trp fluorescence emission of RiLK3 by 5-NS and 16-NS in (**E**) *S.* Typhimurium or (**F**) *S. aureus* MLVs. Q: quencher

Fig. 6. Kinetics of leakage for CF encapsulated in LUVs in response to RiLK1 or RiLK3 addition. The vesicles simulating (**A**) *S.* Typhimurium ($DOPE_{78}$:$POPG_{18}$:CL_4), and (**B**) *S. aureus* (CL_{42}:$POPG_{58}$) were prepared containing 25 mM CF by extrusion, using a polycarbonate porous membrane to render vesicles of 100 nm in size. The removal of free CF outside the vesicles was performed through size-exclusion chromatography (Superdex 30 Increase 10/300 GL column) using 10 mM HEPES, 100 mM NaCl pH 7.2. The fluorescence

emission of CF was monitored in the range from 500 to 600 nm with excitation at λ=490 nm. After 30 min, Triton X-100 (1%) was added to induce complete leakage of CF.

Fig. 7. Dynamic light scattering and ζ-potential analysis of bacterial membrane liposomes. **(A)** Hydrodynamic size distribution of *Salmonella*-like liposomes (0.2 mM) alone (black curve) or interacting with RiLK1 (0.0025, 0.005, 0.01, and 0.1 mM, red, blue, green, and purple curves, respectively). **(B)** Hydrodynamic size distribution of *Salmonella*-like liposomes (0.2 mM) alone (black curve) or interacting with $CaCl_2$ (0.1, 1, and 4.5 mM, red, blue, and green curves, respectively). **(C)** ζ-potential histograms of *Salmonell*a-like liposomes (0.2 mM) alone (orange bar), interacting with RiLK1 (0.0025, 0.005, 0.01, and 0.1 mM, green bars), or with $CaCl_2$ (0.1, 1, and 4.5 mM, violet bars). **(D)** Hydrodynamic size distribution of *Staphylococcus*-like liposomes (0.2 mM) alone (black curve) or interacting with RiLK1 (0.0025, 0.005, 0.01, and 0.1 mM, red, blue, green, and purple curves, respectively). **(E)** Hydrodynamic size distribution of *Staphylococcus*-like liposomes (0.2 mM) alone (black curve) or interacting with $CaCl_2$ (0.1, 1, and 4.5 mM, red, blue, and green curves, respectively). **(F)** ζ-potential histograms of *Staphylococcus*-like liposomes (0.2 mM) alone (orange bar), interacting with RiLK1 (0.0025, 0.005, 0.01, and 0.1 mM, green bars), or with $CaCl_2$ (0.1, 1, and 4.5 mM, violet bars).

Fig. 8. Bacteriostatic effect of RiLK1 and RiLK3 against a MDR *Enterococcus faecium*. Bar graph showing the antibacterial activity of RiLK1 (green bars) and RiLK3 (red bars) against MDR *Enterococcus faecium* at two different starting inocula: (**A**) 5×10^3 cfu/mL and (**B**) 5×10^5 cfu/mL. The bacterial load was recorded at the end of the 18 hours of incubation. The experiment was done in triplicate, and the error bar represents standard deviation of the mean.

Journal Pre-proofs

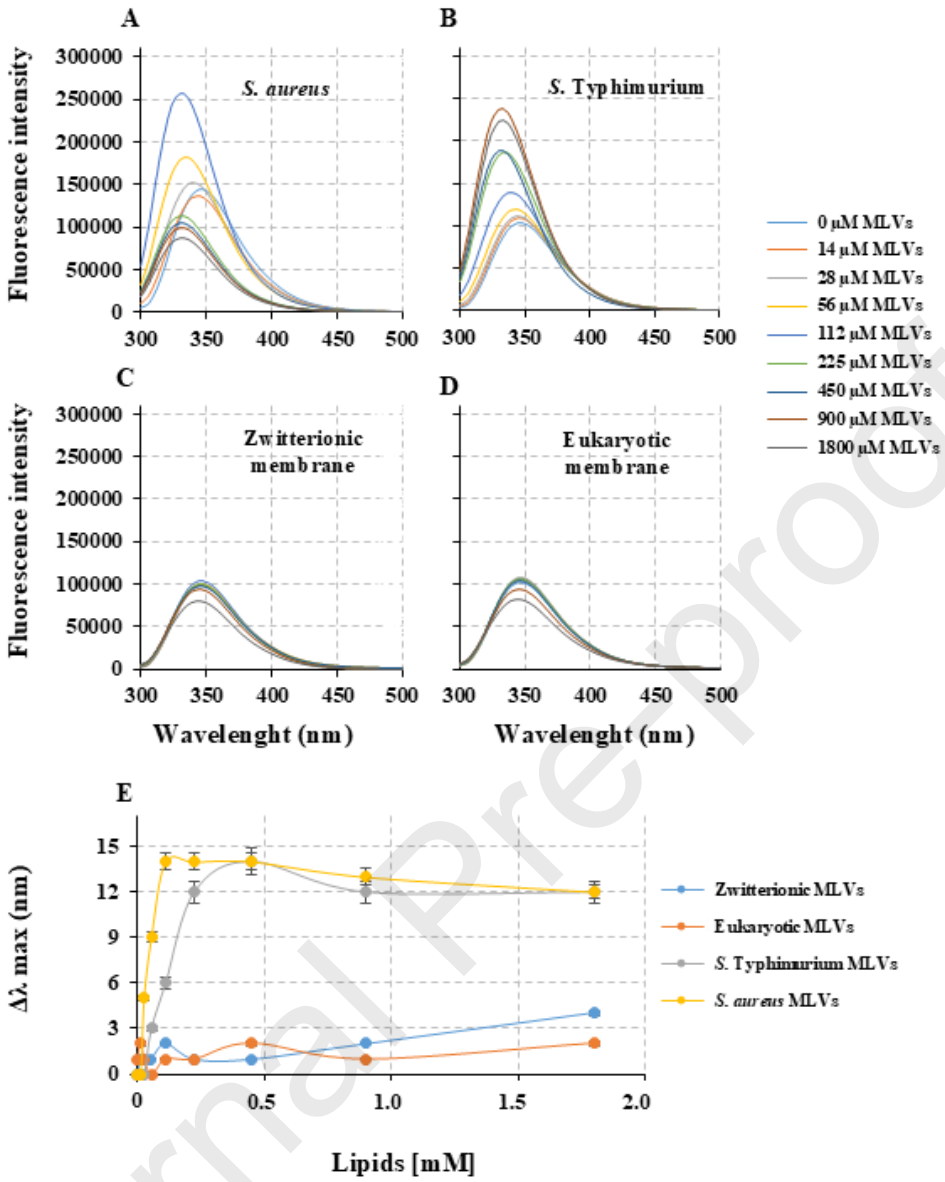

Fig. 1. Changes in Trp fluorescence emission spectra upon the interaction of RiLK1 with MLVs. Fluorescence emission spectra of RiLK1 in the absence (buffer) and presence of increasing concentrations of (**A**) *S. aureus* (CL_{42}:$POPG_{58}$), (**B**) *S.* Typhimurium ($DOPE_{78}$:$POPG_{18}$:CL_4), (**C**) zwitterionic (PC) and (**D**) Eukaryotic (PC_{40}:$POPE_{40}$:SM_{15}:PS_5) multilamellar vesicles (MLVs) obtained upon excitation at 280 nm. **E**) Blue shifts of tryptophan fluorescence emission determined as the difference among the wavelengths at the maximum emission in the absence and presence of lipids ($\Delta\lambda_{max}= \lambda_0 - \lambda$) plotted as a function of lipid concentration. Measurements were performed in 10 mM HEPES, 100 mM NaCl pH 7.2 at 25 °C, using a peptide concentration of 20 µM. All data are presented as the mean (M) ± standard deviation (SD).

Journal Pre-proofs

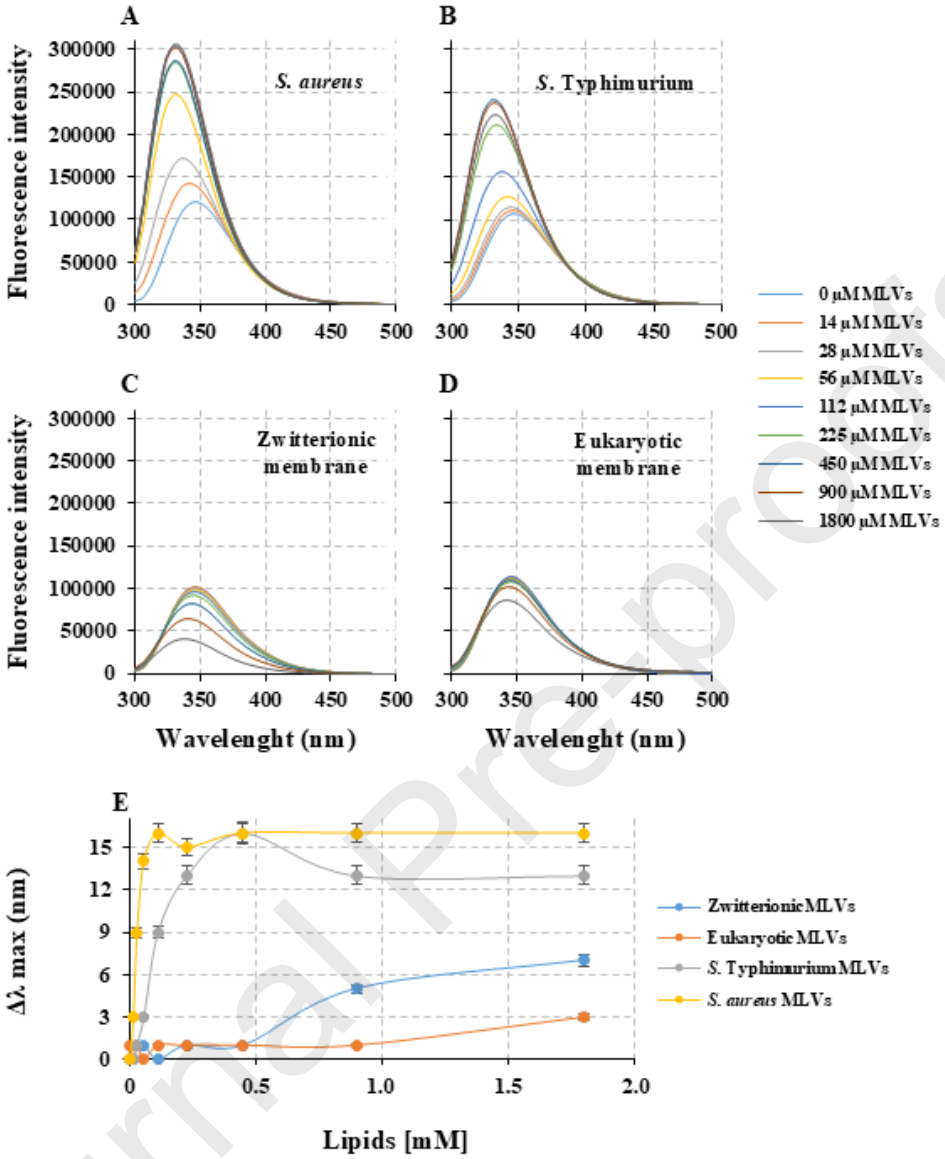

Fig. 2. Changes in Trp fluorescence emission spectra upon the interaction of RiLK3 with MLVs. Fluorescence emission spectra of RiLK3 in the absence (buffer) and presence of increasing concentrations of (**A**) *S. aureus* (CL_{42}:$POPG_{58}$), (**B**) *S.* Typhimurium ($DOPE_{78}$:$POPG_{18}$:CL_4), (**C**) zwitterionic (PC) and (**D**) Eukaryotic (PC_{40}:$POPE_{40}$:SM_{15}:PS_5) multilamellar vesicles (MLVs) obtained upon excitation at 280 nm. **E**) Blue shifts of tryptophan fluorescence emission determined as the difference among the wavelengths at the maximum emission in the absence and presence of lipids ($\Delta\lambda_{max} = \lambda_0 - \lambda$) plotted as a function of lipid concentration. Measurements were performed in 10 mM HEPES, 100 mM NaCl pH 7.2, using a peptide concentration of 20 µM. All data are presented as the mean (M) ± standard deviation (SD).

Journal Pre-proofs

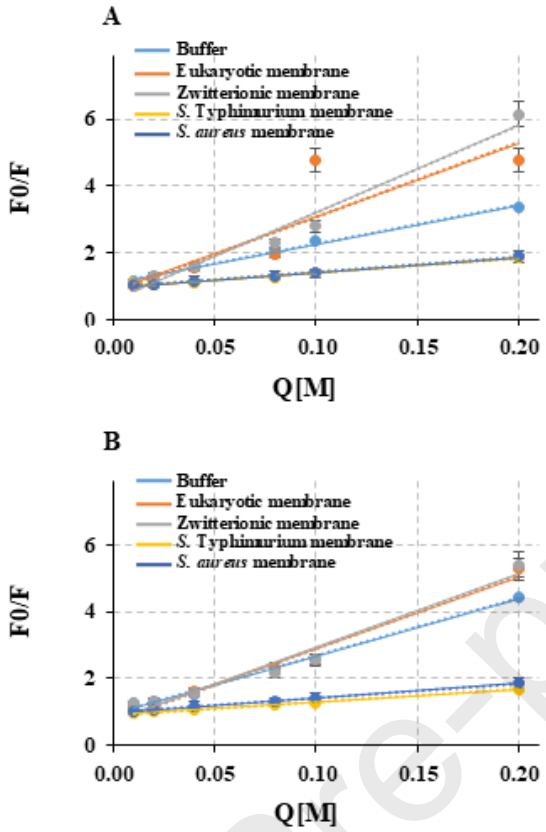

Fig. 3. Acrylamide quenching and Ksv determination. **(A)** Stern-Volmer plots for the quenching of the Trp fluorescence emission of RiLK1 by acrylamide (Q) in buffer and in the presence of differently charged multilamellar vesicles. (**B**) Stern-Volmer plots for the quenching of the Trp fluorescence emission of RiLK3 by acrylamide in buffer and in the presence of differently charged multilamellar vesicles. 1.0 µM of RiLK1 or RiLK3 was incubated in the absence and presence of 30 µM lipid vesicles. The spectra were acquired after 30 minutes of peptide-MLVs incubation. Experimental data was fitted to the Stern-Volmer equation.

Journal Pre-proofs

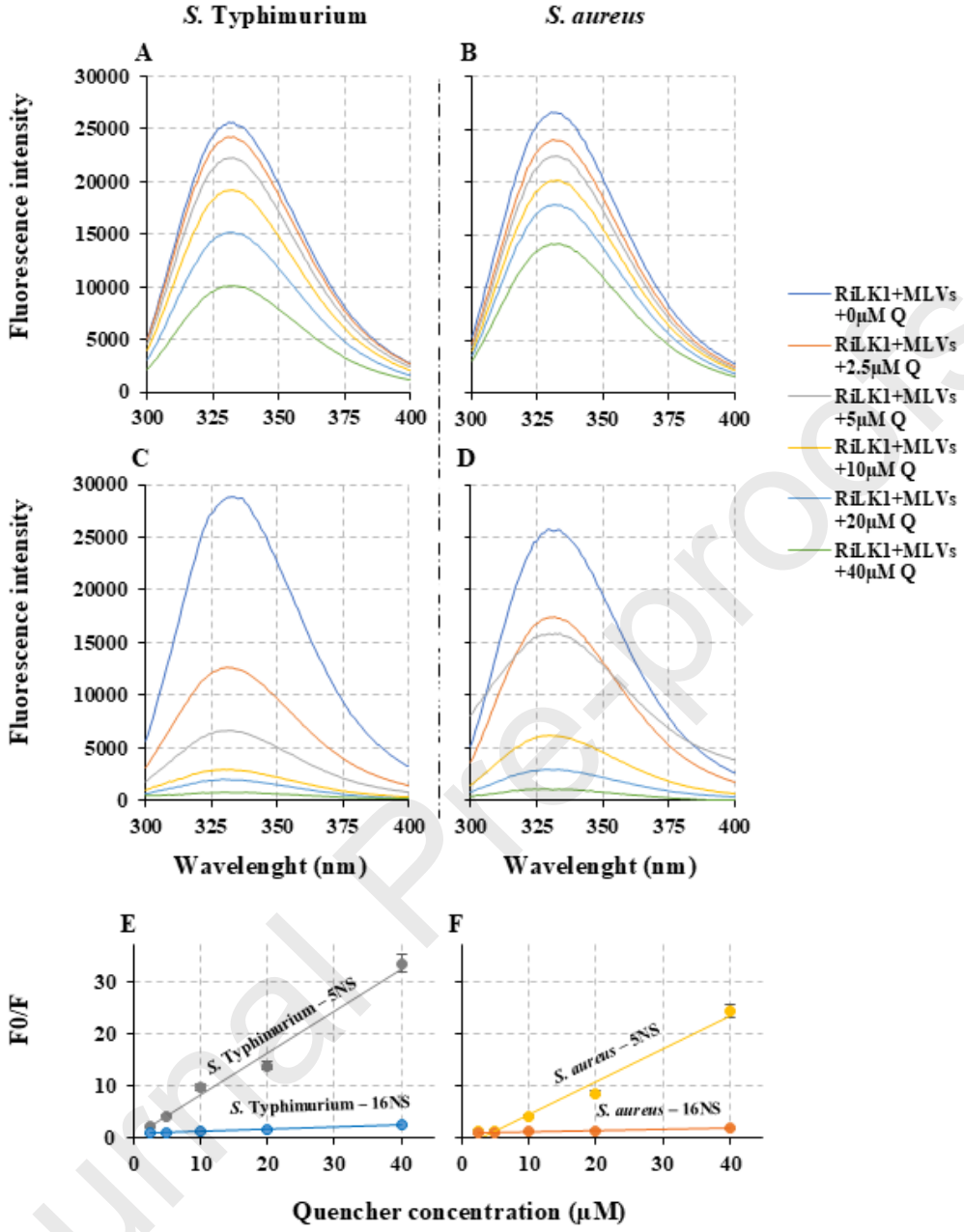

Fig. 4. Emission fluorescence quenching by 16-NS e 5-NS of RiLK1 in bacterial MLVs. Tryptophan fluorescence emission spectra of RiLK1 with increasing concentrations of 16-NS (2.5-40 µM) in the presence of (**A**) *S.* Typhimurium ($DOPE_{78}$:$POPG_{18}$:CL_4), or (**B**) S. *aureus* (CL_{42}:$POPG_{58}$). Tryptophan fluorescence emission spectra of RiLK1 with increasing concentrations of 5-NS (2.5-40 µM) in the presence of (**C**) *S.* Typhimurium ($DOPE_{78}$:$POPG_{18}$:CL_4) or (**D**) S. *aureus* (CL_{42}:$POPG_{58}$). Stern-Volmer plots of the quenching of the Trp fluorescence emission of RiLK1 by 5-NS and 16-NS in (**E**) *S.* Typhimurium or (**F**) *S. aureus* MLVs. Q: quencher

Journal Pre-proofs

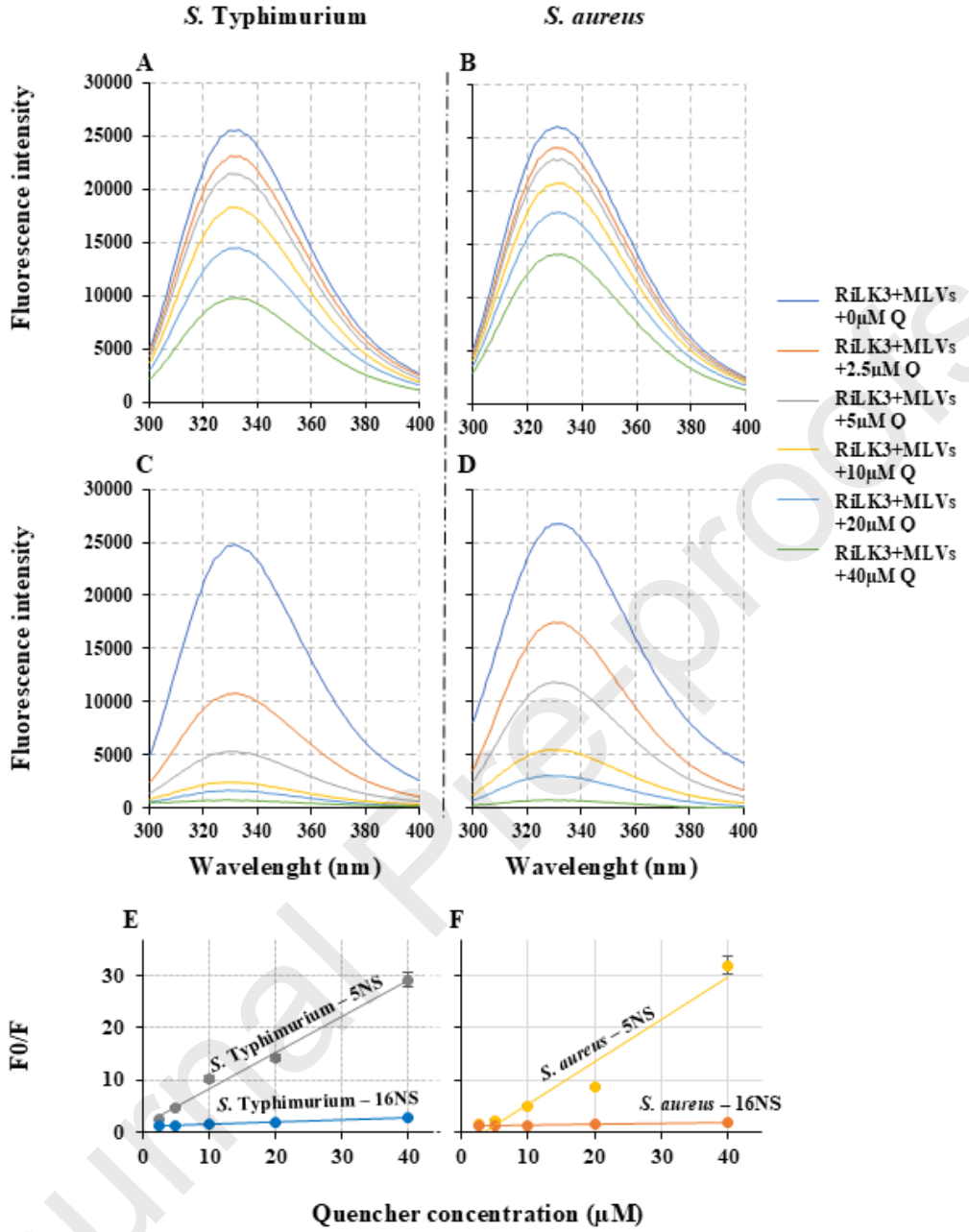

Fig. 5. Emission fluorescence quenching by 16-NS e 5-NS of RiLK3 in bacterial MLVs. Tryptophan fluorescence emission spectra of RiLK3 with increasing concentrations of 16-NS (2.5-40 μM) in the presence of (**A**) *S.* Typhimurium ($DOPE_{78}$:$POPG_{18}$:CL_4), or (**B**) S. *aureus* (CL_{42}:$POPG_{58}$). Tryptophan fluorescence emission spectra of RiLK3 with increasing concentrations of 5-NS (20-100 μM) in the presence of (**C**) *S.* Typhimurium ($DOPE_{78}$:$POPG_{18}$:CL_4), and (**D**) S. *aureus* (CL_{42}:$POPG_{58}$). Stern-Volmer plots of the quenching of the Trp fluorescence emission of RiLK3 by 5-NS and 16-NS in (**E**) *S.* Typhimurium or (**F**) *S. aureus* MLVs. Q: quencher

Journal Pre-proofs

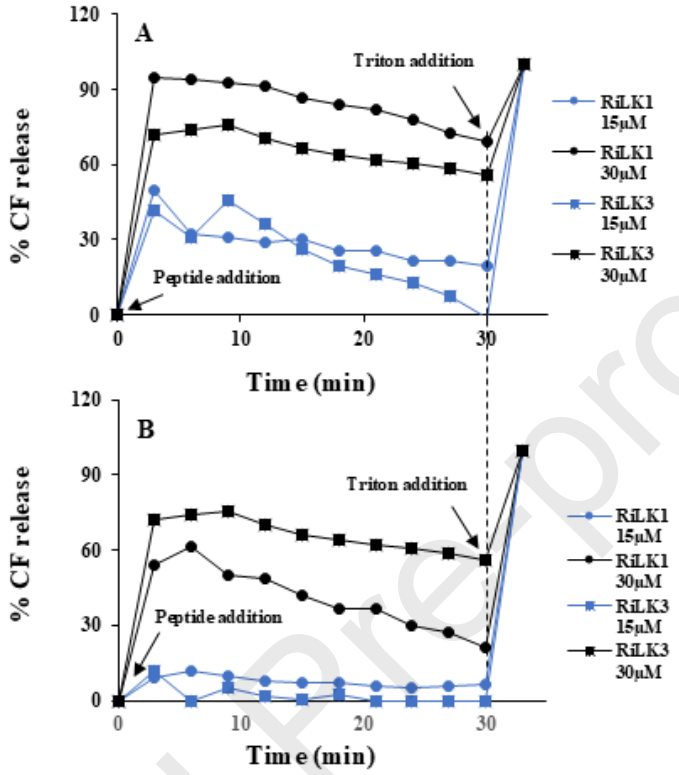

Fig. 6. Kinetics of leakage for CF encapsulated in LUVs in response to RiLK1 or RiLK3 addition. The vesicles simulating (**A**) *S.* Typhimurium ($DOPE_{78}$:$POPG_{18}$:CL_4), and (**B**) *S. aureus* (CL_{42}:$POPG_{58}$) were prepared containing 25 mM CF by extrusion, using a polycarbonate porous membrane to render vesicles of 100 nm in size. The removal of free CF outside the vesicles was performed through size-exclusion chromatography (Superdex 30 Increase 10/300 GL column) using 10 mM HEPES, 100 mM NaCl pH 7.2. The fluorescence emission of CF was monitored in the range from 500 to 600 nm with excitation at λ=490 nm. After 30 min, Triton X-100 (1%) was added to induce complete leakage of CF.

Journal Pre-proofs

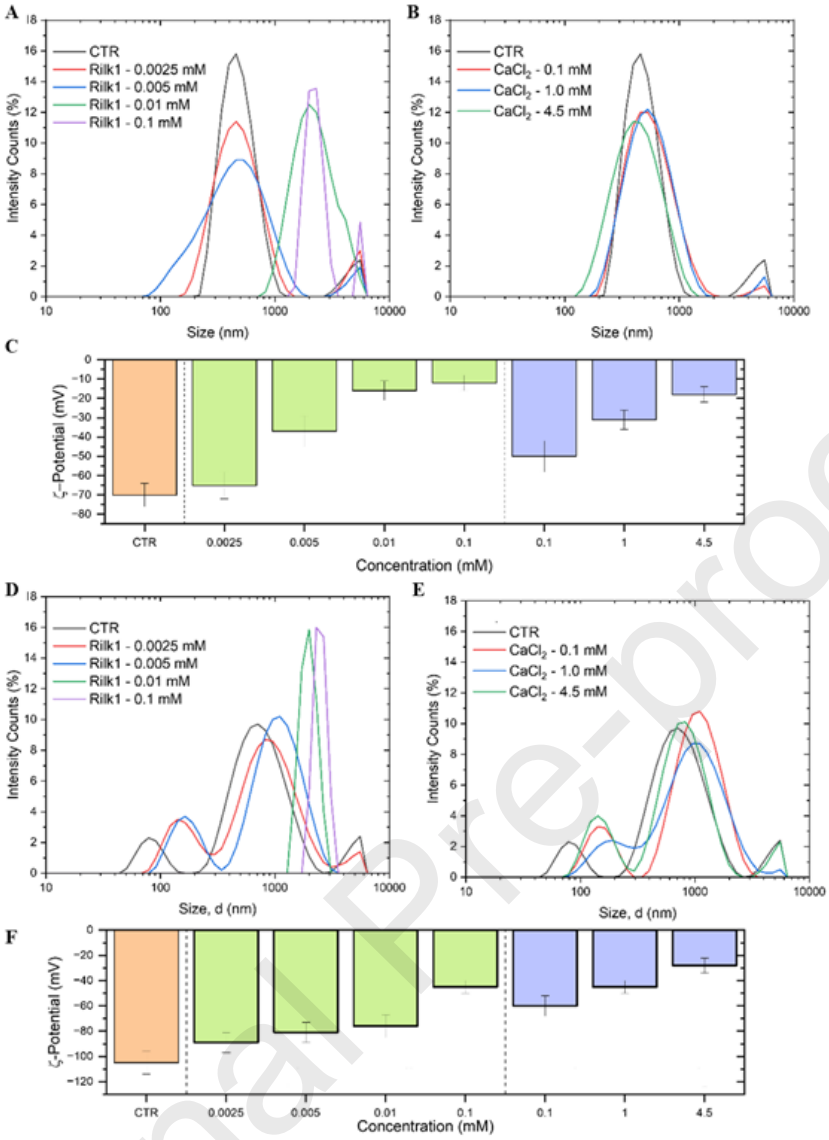

Fig. 7. Dynamic light scattering and ζ-potential analysis of bacterial membrane liposomes. (**A**) Hydrodynamic size distribution of *Salmonella*-like liposomes (0.2 mM) alone (black curve) or interacting with RiLK1 (0.0025, 0.005, 0.01, and 0.1 mM, red, blue, green, and purple curves, respectively). (**B**) Hydrodynamic size distribution of *Salmonella*-like liposomes (0.2 mM) alone (black curve) or interacting with $CaCl_2$ (0.1, 1, and 4.5 mM, red, blue, and green curves, respectively). (**C**) ζ-potential histograms of *Salmonella*-like liposomes (0.2 mM) alone (orange bar), interacting with RiLK1 (0.0025, 0.005, 0.01, and 0.1 mM, green bars), or with $CaCl_2$ (0.1, 1, and 4.5 mM, violet bars). (**D**) Hydrodynamic size distribution of *Staphylococcus*-like liposomes (0.2 mM) alone (black curve) or interacting with RiLK1 (0.0025, 0.005, 0.01, and 0.1 mM, red, blue, green, and purple curves, respectively). (**E**) Hydrodynamic size distribution of *Staphylococcus*-like liposomes (0.2 mM) alone (black curve) or interacting with $CaCl_2$ (0.1, 1, and 4.5 mM, red, blue, and green curves, respectively). (**F**) ζ-potential histograms of *Staphylococcus*-like liposomes (0.2 mM) alone (orange bar), interacting with RiLK1 (0.0025, 0.005, 0.01, and 0.1 mM, green bars), or with $CaCl_2$ (0.1, 1, and 4.5 mM, violet bars).

Journal Pre-proofs

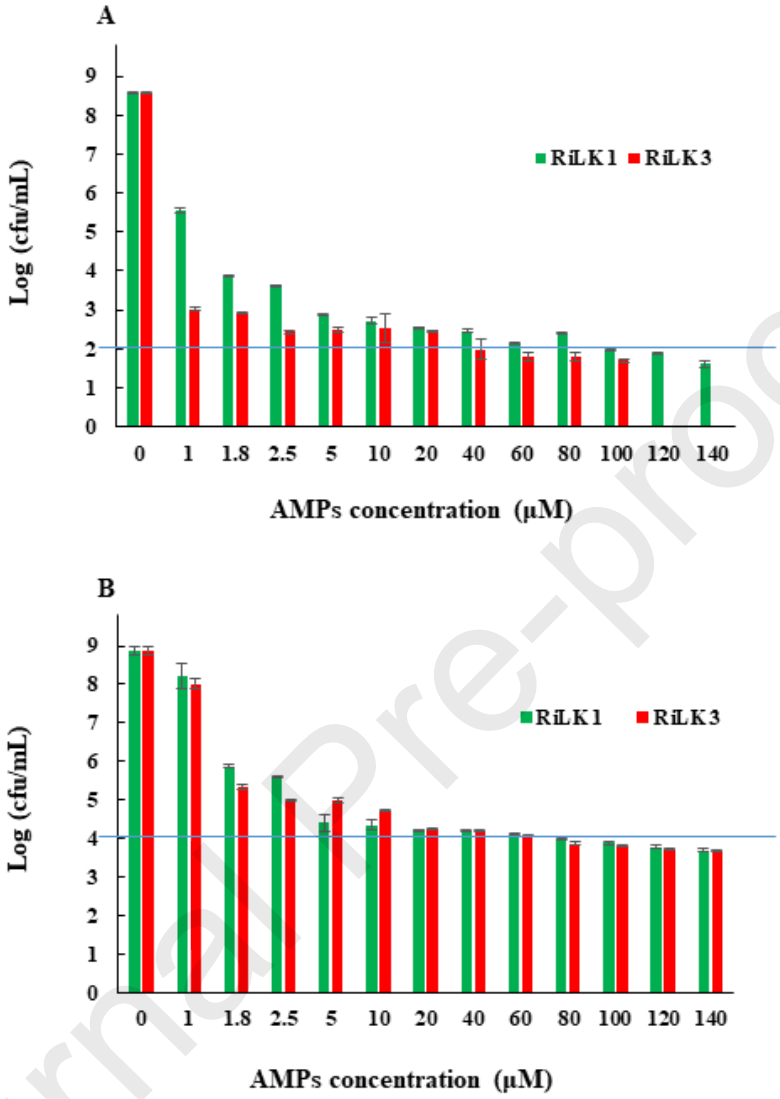

Fig. 8. Bacteriostatic effect of RiLK1 and RiLK3 against a MDR *Enterococcus faecium*. Bar graph showing the antibacterial activity of RiLK1 (green bars) and RiLK3 (red bars) against MDR *Enterococcus faecium* at two different starting inocula: (**A**) 5×10^3 cfu/mL and (**B**) 5×10^5 cfu/mL. The bacterial load was recorded at the end of the 18 hours of incubation. The experiment was done in triplicate, and the error bar represents standard deviation of the mean.

Table 1. Stern–Volmer constants (Ksv) and Normalized Accessibility Factor (NAF) obtained from acrylamide quenching studies of Trp fluorescence of RiLK-peptides in the absence or presence of differently charged vesicles. NAF is defined in the text and the Ksv values were calculated using the Stern-Volmer equation (1).

Journal Pre-proofs

		Buffer	Zwitterionic membrane	Eukaryotic membrane	*S.* Typhimurium	*S. aureus*
Ksv (M^{-1})	*RiLK1*	11.6 ± 0.7	26.2 ± 1.4	22.2 ± 1.8	4.3 ± 0.1	4.5 ± 0.1
	RiLK3	17.2 ± 0.8	22.0 ± 1.3	21.6 ± 1.1	3.7 ± 0.1	4.3 ± 0.1
NAF	*RiLK1*	1	2.3 ± 0.1	1.9 ± 0.1	0.4 ± 0.0	0.4 ± 0.0
	RiLK3	1	1.3 ± 0.1	1.3 ± 0.1	0.3 ± 0.0	0.3 ± 0.0

Journal Pre-proofs

Table 2. Stern–Volmer constants (K_{SV}) obtained for the RiLK-peptides in bacterial MLVs, quenched by 16-NS and 5-NS, using Equation (1). Data are presented as the best-fit value from three independent experiments ± SD.

RiLK1	Lipid vesicles	System	K_{SV} (mM^{-1}) 16-NS	K_{SV} (mM^{-1}) 5-NS
	S. Typhimurium	$DOPE_{78}$:$POPG_{18}$:CL_4	39.4 ± 1.3	809.3 ± 27.4
	S. aureus	CL_{42}:$POPG_{58}$	20.0 ± 0.7	622.2 ± 19.1

RiLK3	Lipid vesicles	System	K_{SV} (mM^{-1}) 16-NS	K_{SV} (mM^{-1}) 5-NS
	S. Typhimurium	$DOPE_{78}$:$POPG_{18}$:CL_4	39.8 ± 1.0	693.4 ± 16.8
	S. aureus	CL_{42}:$POPG_{58}$	20.5 ± 0.6	810.2 ± 29.5

Journal Pre-proofs

Starting inoculum	RiLK1	RiLK3
5×10^3 cfu/mL	1.8 μM	1.0 μM
5×10^5 cfu/mL	2.5 μM	1.8 μM

Table 3. MIC values of RiLK1 and RiLK3 against *Enterococcus faecium* at two starting inoculum concentrations

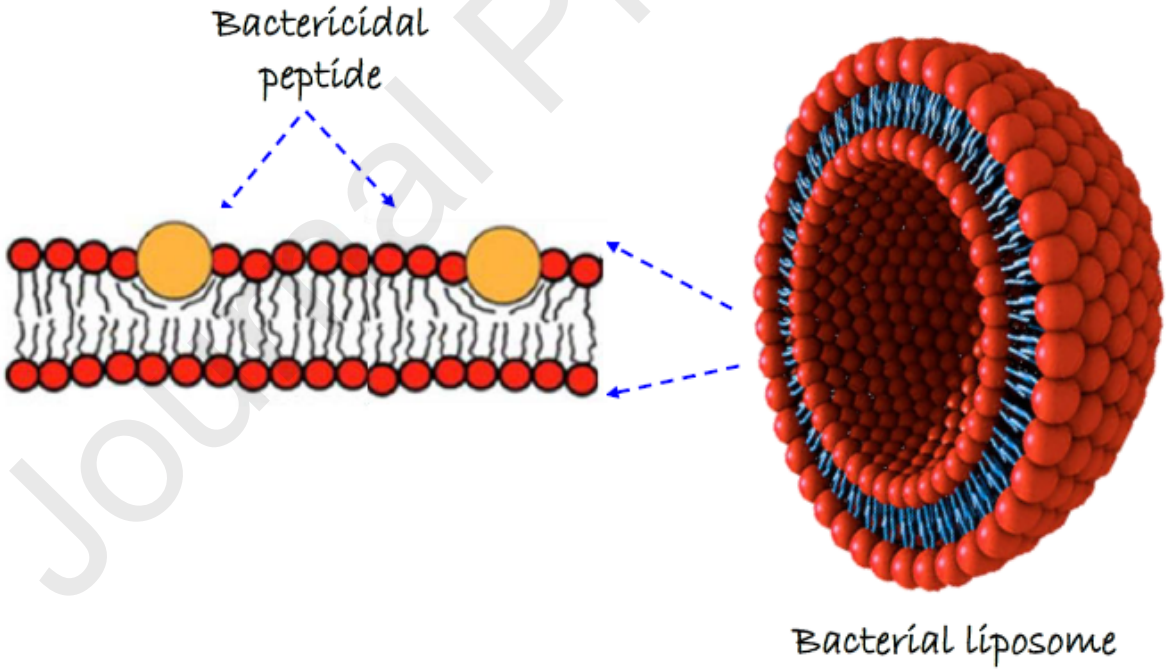

Journal Pre-proofs

Highlights

- RiLK1 and RiLK3 belong to the class of membrane-active antimicrobial peptides
- RiLK-peptides have the potential to combat MDR *Enterococcus faecium* strain.

- RiLK-peptides are mainly located at the interface of the negatively charged membranes.

Journal Pre-proofs